

Studying the $b \rightarrow s\ell^+\ell^-$ anomalies and $(g-2)_\mu$ in R -parity violating MSSM framework with the inverse seesaw mechanism

Min-Di Zheng^{*} and Hong-Hao Zhang[†]

School of Physics, Sun Yat-Sen University, Guangzhou 510275, China

Abstract

Inspired by the recent experimental results which show deviations from the standard model (SM) predictions of $b \rightarrow s\ell^+\ell^-$ transitions, we study the R -parity violating minimal supersymmetric standard model (RPV-MSSM) extended by the inverse seesaw mechanism. The trilinear R -parity violating terms, together with the chiral mixing of sneutrinos, induce the loop contributions to the $b \rightarrow s\ell^+\ell^-$ anomaly. We study the parameter space of the single-parameter scenario $C_{9,\mu}^{\text{NP}} = -C_{10,\mu}^{\text{NP}} = C_V$ and the double-parameter scenario (C_V, C_U) , respectively, constrained by other experimental data such as $B_s - \bar{B}_s$ mixing, $B \rightarrow X_s \gamma$ decay, the lepton flavour violating decays, etc. Both the single-parameter and the double-parameter scenario can resolve the long existing muon anomalous magnetic moment problem as well, and allow the anomalous $t \rightarrow c g$ process to reach the sensitivity at the Future Circular hadron-hadron Collider (FCC-hh).

^{*}zhengmd5@mail.sysu.edu.cn

[†]zhh98@mail.sysu.edu.cn

1 Introduction

In recent years, several hints of new physics (NP) beyond the SM have shown up, such as, $R_{K^{(*)}} = \mathcal{B}(B \rightarrow K^{(*)}\mu^+\mu^-)/\mathcal{B}(B \rightarrow K^{(*)}e^+e^-)$ on the transitions of $b \rightarrow s\ell^+\ell^-$ ($\ell = e, \mu$), which exhibits the very attractive anomalies. Especially, the measurement of R_K by the LHCb Collaboration has just been updated with the full run II data as $R_K = 0.846_{-0.039}^{+0.042} {}_{-0.012}^{+0.013}$ in the q^2 bin $[1.1, 6]$ GeV² [1], which is much more precise than the previous one $R_K = 0.846_{-0.054}^{+0.060} {}_{-0.014}^{+0.016}$ [2], giving rise to the discrepancy with the SM value changing from preceding 2.5σ to 3.1σ . The recent measurements of R_{K^*} by LHCb give $R_{K^*} = 0.66_{-0.07}^{+0.11} \pm 0.03$ at $[0.045, 1.1]$ GeV² bin and $R_{K^*} = 0.69_{-0.07}^{+0.11} \pm 0.05$ at $[1.1, 6]$ GeV² bin, showing 2.1σ deviation at low q^2 region and 2.5σ deviation at high region, respectively [3]. The $R_{K^{(*)}}$ results by the Belle Collaboration [4, 5] show the consistency with the SM predictions although the results have sizable experimental error bars. Besides, there are also other anomalies in the $b \rightarrow s\ell^+\ell^-$ transition, for instance, the angular observable P'_5 anomaly of $B \rightarrow K^*\mu^+\mu^-$ decay persists with the new data [6] compared with the run I results [7–12]. All these anomalies may indicate the NP that breaks lepton flavour universality (LFU).

One knows that each single anomaly above cannot be regarded as the conclusive evidence of NP. However, it is interesting that nearly all these anomalies can be explained simultaneously with the four-Fermi operators in the model-independent global fit [13–36]. In light of the new measurement of R_K [1], there are already some new fit results updated [14, 23–36]. For the discussion of the global fit, the related Lagrangian of low energy effective field theory is given by

$$\mathcal{L}_{\text{eff}} = \frac{4G_F}{\sqrt{2}}\eta_t \sum_i C_i \mathcal{O}_i + \text{h.c.}, \quad (1.1)$$

where the Cabibbo–Kobayashi–Maskawa (CKM) factor $\eta_t \equiv K_{tb}K_{ts}^*$. The main operators for the anomaly explanations are

$$\mathcal{O}_9 = \frac{e^2}{16\pi^2}(\bar{s}\gamma_\mu P_L b)(\bar{\ell}\gamma^\mu \ell), \quad \mathcal{O}_{10} = \frac{e^2}{16\pi^2}(\bar{s}\gamma_\mu P_L b)(\bar{\ell}\gamma^\mu \gamma_5 \ell), \quad (1.2)$$

where $P_L = (1 - \gamma_5)/2$ is the left-handed (LH) chirality projector and the Wilson coefficients $C_{9(10)} = C_{9(10)}^{\text{SM}} + C_{9(10)}^{\text{NP}}$. In this work, we adopt the following unified form of fit scenarios

$$C_{9,\mu}^{\text{NP}} = C_V + C_U, \quad C_{10,\mu}^{\text{NP}} = -C_V,$$

$$C_{9,e}^{\text{NP}} = C_U, \quad C_{10,e}^{\text{NP}} = 0, \quad (1.3)$$

where V denotes the contributions only of $\mu^+\mu^-$ channel and U denotes LFU contributions. The first scenario, called scenario A here, requires $C_U = 0$ to realize the single-parameter scenario $C_{9,\mu}^{\text{NP}} = -C_{10,\mu}^{\text{NP}}$ in fact. We adopt the fit result $-0.46 < C_V < -0.32$ that conforms to the rare B -meson decays at 1σ level in Ref. [28]. Except the new R_K measurement [1], authors in Ref. [28] have also considered other series of new experimental results, such as the new angular analyses of $B^0 \rightarrow K^{*0}\mu^+\mu^-$ [6] and $B^\pm \rightarrow K^{*\pm}\mu^+\mu^-$ [37], the updated branching ratio measurement of the $B_s \rightarrow \phi\mu^+\mu^-$ [38] that confirms the previous tension [39] with the SM prediction, as well as the recent results of $B_s \rightarrow \mu^+\mu^-$ from CMS [40] and LHCb [41, 42]. For the case of $C_U \neq 0$, named as scenario B, we also utilize the fit regions in Ref. [28] with the best fit point $(C_V, C_U) \approx (-0.34, -0.32)$.

After these results of the model-independent analyses are obtained, imperative works are to find the concrete NP models which can conform to them. Both the scenario A and B have been implemented in RPV-MSSM [43–48]. When masses of sneutrinos/sd-quarks are sufficiently heavy or there is a cancellation in the penguin contribution [46], the scenario B turns into the scenario A.

More than RPV-MSSM, the seesaw mechanism [49–55] is also researched for the explanation of $b \rightarrow s\ell^+\ell^-$ disparities in the supersymmetric (SUSY) models [56], two-Higgs doublet [57, 58] and other frameworks (see Refs. [59–73] e.g.). The seesaw mechanism is one of the most attractive methods to generate the neutrino masses in accord with the conclusive evidence of neutrino oscillations [74]. As one type of seesaw mechanisms, the inverse seesaw [75, 76] can give a $\mathcal{O}(1)$ neutrino Yukawa coupling Y_ν . The relative large Y_ν implicates that the admixture between LH neutrino superfields and right-handed (RH) or extra singlet ones is not negligible. Therefore, it is meaningful to study the chiral mixings of (s)neutrinos in MSSM framework extended by both inverse seesaw mechanisms and the tree-level trilinear RPV terms, and then all chiral parts of (s)neutrinos more than LH ones can interact with (s)quarks. This new combination is naturally reasonable [77–79] and has never been studied in the $b \rightarrow s\ell^+\ell^-$ anomalies to our knowledge.

The recent experimental results of $R(D^{(*)}) = \mathcal{B}(B \rightarrow D^{(*)}\tau\nu)/\mathcal{B}(B \rightarrow D^{(*)}\ell\nu)$ in charged current $b \rightarrow c\tau\nu$ from BaBar [80, 81], Belle [82–85] and LHCb [86–88] have been averaged by the Heavy Flavor Averaging Group [89], and also show the tension with the average of SM

predictions [90–93] and the recent new SM results [94–99]. While the new measurements of $R(D^{(*)})$ from Belle using the semileptonic tagging method, such as the latest results with the data sample of 772×10^6 $B\bar{B}$ pairs, are already in agreement with SM predictions well, and Belle combined results are consistent with SM predictions within 1.6σ [100]. Given this, in this work, we do not investigate $R(D^{(*)})$ for the moment.

The clues of LFU violation exist not only in B -meson decays but also in other processes, such as, the muon anomalous magnetic moment problem which has existed for several decades. The measurement of $a_\mu = (g - 2)_\mu$ by Fermilab [101–103] presents the 3.3σ deviation greater than the SM prediction [104]¹, and agrees with the previous Brookhaven E821 experiment [114]. The combined deviation average of the two experiments, $\Delta a_\mu = a_\mu^{\text{exp}} - a_\mu^{\text{SM}} = (2.51 \pm 0.59) \times 10^{-9}$ shows the increased tension at the significant 4.2σ level and this is a growing motivation of NP. For the electron anomalous magnetic moment, there is a negative 2.4σ discrepancy between the measurement [115] and the SM prediction [116], $\Delta a_e = a_e^{\text{exp}} - a_e^{\text{SM}} = (-8.7 \pm 3.6) \times 10^{-13}$, due to the new measurement of the fine structure constant in Ref. [117]². There are plentiful articles discussing the $(g - 2)_\mu$ problem in the SUSY framework (e.g., see Refs. [48, 120–169]). In this work, we will investigate whether the parameter space for the explanation of $b \rightarrow s\ell^+\ell^-$ anomalies can be in accord with the deviation Δa_μ , and then discuss the NP effects on a_e .

Our paper is organized as follows. At first, the new model in this work is introduced in section 2. Then in section 3, the whole one-loop contributions to the $b \rightarrow s\ell^+\ell^-$ transition in this model are scrutinized and we emphasize the main contributions to explain the $b \rightarrow s\ell^+\ell^-$ anomaly in our parameter scheme. We discuss NP contributions to $(g - 2)_\ell$ and other related constraints in section 4 followed by the numerical results and discussions in section 5. Our conclusions are presented in section 6.

¹A recent calculation of the hadronic vacuum polarization (HVP) [105] weakens the discrepancy between the experiment and SM prediction of a_μ while it shows the tension with the R-ratio determinations [106–109]. And even the large HVP contribution can account for the measurement of a_μ , there exists the tension within the electroweak (EW) fit [110–113]. We do not consider this HVP result here but consider the preceding review of various SM results [104].

²Another new measurement of the fine structure constant [118] differs by more than 5σ to the previous one [117] and affects the deviation Δa_e to positive 1.6σ level [119]. The NP hint search in a_e still expects more experimental researches and we focus on a_μ anomaly explanations in this work.

2 The Model

The model considered in this work is RPV-MSSM with inverse seesaw mechanisms called RPV-MSSMIS here and the superpotential is expressed by

$$\mathcal{W} = \mathcal{W}_{\text{MSSM}} + Y_\nu^{ij} \hat{R}_i \hat{L}_j \hat{H}_u + M_R^{ij} \hat{R}_i \hat{S}_j + \frac{1}{2} \mu_S^{ij} \hat{S}_i \hat{S}_j + \lambda'_{ijk} \hat{L}_i \hat{Q}_j \hat{D}_k, \quad (2.1)$$

where the generation indices $i, j, k = 1, 2, 3$ while the colour ones are omitted. All the repeated indices are defaulted to be summed over unless otherwise stated. Here the superpotential of MSSM [170, 171] is expressed as

$$\mathcal{W}_{\text{MSSM}} = \mu \hat{H}_u \hat{H}_d + Y_u^{ij} \hat{U}_i \hat{Q}_j \hat{H}_u - Y_d^{ij} \hat{D}_i \hat{Q}_j \hat{H}_d - Y_e^{ij} \hat{E}_i \hat{L}_j \hat{H}_d. \quad (2.2)$$

In RPV-MSSMIS, MSSM superfields are extended by three generations of pairs of SM singlet superfields, \hat{R}_i and \hat{S}_i . The neutral parts of two Higgs doublet superfields $\hat{H}_u = (\hat{H}_u^+, \hat{H}_u^0)^T$ and $\hat{H}_d = (\hat{H}_d^0, \hat{H}_d^-)^T$ acquire the non-zero vacuum expectation values, $\langle \hat{H}_u^0 \rangle = v_u$ and $\langle \hat{H}_d^0 \rangle = v_d$ respectively, leading to the mixing angle $\beta = \tan^{-1}(v_u/v_d)$. The tree-level trilinear RPV coupling $\lambda'_{ijk} \hat{L}_i \hat{Q}_j \hat{D}_k$ can be added for \hat{L}_i sharing the same SM quantum number with \hat{H}_d . It is needed to point out that the RPV superpotential terms like $\lambda'_{ijk} \hat{L}_i \hat{Q}_j \hat{D}_k$, $\lambda_{ijk} \hat{L}_i \hat{L}_j \hat{E}_k$, $\lambda''_{ijk} \hat{U}_i \hat{D}_j \hat{D}_k$ as well as $\mu_i \hat{L}_i \hat{H}_u$ are all in principle allowed for the SM gauge invariance if there are no extra symmetries. Here we only consider the term $\lambda'_{ijk} \hat{L}_i \hat{Q}_j \hat{D}_k$ connecting the quark sector with lepton sector, without the pure-quark term $\lambda''_{ijk} \hat{U}_i \hat{D}_j \hat{D}_k$ or the purely lepton interaction $\lambda_{ijk} \hat{L}_i \hat{L}_j \hat{E}_k$, because of the attempt to avoid the probable disastrously rapid proton decay [172, 173] when there are nonzero parameters λ' and λ'' simultaneously and the strong collider constraints on the lightest sneutrino mass when the λ' and λ both exist [174–184]. The bilinear term $\mu_i \hat{L}_i \hat{H}_u$ is also allowed but we exclude it in order to avoid the extra contributions to neutrino masses [185]. With the scalar components of Higgs doublet superfields denoted by H_u and H_d , and squarks and sleptons denoted by “ $\tilde{}$ ”, the soft supersymmetry breaking Lagrangian is given by

$$\begin{aligned} -\mathcal{L}^{\text{soft}} = & -\mathcal{L}_{\text{MSSM}}^{\text{soft}} + (m_{\tilde{R}}^2)_{ij} \tilde{R}_i^* \tilde{R}_j + (m_{\tilde{S}}^2)_{ij} \tilde{S}_i^* \tilde{S}_j \\ & + (A_\nu Y_\nu)_{ij} \tilde{R}_i^* \tilde{L}_j H_u + B_{M_R}^{ij} \tilde{R}_i^* \tilde{S}_j + \frac{1}{2} B_{\mu_S}^{ij} \tilde{S}_i \tilde{S}_j, \end{aligned} \quad (2.3)$$

where $\mathcal{L}_{\text{MSSM}}^{\text{soft}}$ corresponds to MSSM part [170, 171]. It should be mentioned that MSSM and singlet neutrino sectors are all at low scale (around 1 TeV) in this work, so some terms in the most general superpotential and soft breaking Lagrangian are already or will be eliminated ad hoc for the phenomenological consideration.

As to the three terms following $\mathcal{W}_{\text{MSSM}}$ in Eq. (2.1) which give the neutrino mass spectrum at tree level, the 9×9 mass matrix of neutrino in the (ν, R, S) basis is given by

$$\mathcal{M}_\nu = \begin{pmatrix} 0 & m_D^T & 0 \\ m_D & 0 & M_R \\ 0 & M_R^T & \mu_S \end{pmatrix}, \quad (2.4)$$

in which $m_D = \frac{1}{\sqrt{2}}v_u Y_\nu^T$. And the μ_S parameter can be obtained by

$$\mu_S = (m_D^T)^{-1} M_R U_{\text{PMNS}} m_\nu^{\text{diag}} U_{\text{PMNS}}^T M_R^T m_D^{-1}, \quad (2.5)$$

when $\mu_S \ll m_D < M_R$. The diagonalized neutrino mass $\mathcal{M}_\nu^{\text{diag}}$ in physics basis containing the three-light-generation part m_ν^{diag} in Eq. (2.5), is given by $\mathcal{M}_\nu^{\text{diag}} = \mathcal{V} \mathcal{M}_\nu \mathcal{V}^T$. Here embedded in the whole 9×9 mixing matrix \mathcal{V}^T , the 3×3 light-generation sector $\mathcal{V}_{3 \times 3}^T$ should approximate the PMNS matrix U^{PMNS} [74, 186].

Then we turn to the sneutrino mass square matrix in the $(\tilde{\nu}_L^{\mathcal{I}(\mathcal{R})}, \tilde{R}^{\mathcal{I}(\mathcal{R})}, \tilde{S}^{\mathcal{I}(\mathcal{R})})$ basis, which is expressed as

$$\mathcal{M}_{\tilde{\nu}^{\mathcal{I}(\mathcal{R})}}^2 = \begin{pmatrix} m_{\tilde{L}'}^2 & (A_\nu - \mu \cot \beta) m_D^T & m_D^T M_R \\ (A_\nu - \mu \cot \beta) m_D & m_R^2 + M_R M_R^T + m_D m_D^T & \pm M_R \mu_S + B_{M_R} \\ M_R^T m_D & \pm \mu_S M_R^T + B_{M_R}^T & m_{\tilde{S}}^2 + \mu_S^2 + M_R^T M_R \pm B_{\mu_S} \end{pmatrix}, \quad (2.6)$$

where the “ \pm ” above expresses the CP -even and CP -odd, and also CP -odd is denoted by \mathcal{I} and CP -even is denoted by \mathcal{R} . The soft mass $m_{\tilde{L}'}^2 = m_{\tilde{L}}^2 + \frac{1}{2} m_Z^2 \cos 2\beta + m_D m_D^T$ can be regarded as one whole input where $m_{\tilde{L}}^2$ is the soft mass square of \tilde{L} in $\mathcal{L}_{\text{MSSM}}^{\text{soft}}$. The CP -even and CP -odd masses can be nearly the same for tiny μ_S and relatively small B_{μ_S} [187]. Besides, the value of

$m_{\tilde{S}}^2$ is set to be zero here. Thus, the approximate form is provided as [188]

$$\mathcal{M}_{\tilde{\nu}^{\mathcal{I}(\mathcal{R})}}^2 \approx \begin{pmatrix} m_{\tilde{L}'}^2 & (A_\nu - \mu \cot \beta) m_D^T & m_D^T M_R \\ (A_\nu - \mu \cot \beta) m_D & m_{\tilde{R}}^2 + M_R M_R^T + m_D m_D^T & B_{M_R} \\ M_R^T m_D & B_{M_R}^T & M_R^T M_R \end{pmatrix}. \quad (2.7)$$

In the following we adopt this particular structure and then the mixing matrices $\tilde{\mathcal{V}}^{\mathcal{I}(\mathcal{R})}$, which diagonalize sneutrino mass square matrices by $\tilde{\mathcal{V}}^{\mathcal{I}(\mathcal{R})} \mathcal{M}_{\tilde{\nu}^{\mathcal{I}(\mathcal{R})}}^2 \tilde{\mathcal{V}}^{\mathcal{I}(\mathcal{R})\dagger} = (\mathcal{M}_{\tilde{\nu}^{\mathcal{I}(\mathcal{R})}}^2)^{\text{diag}}$, are also the same whether CP even or odd. All the $\tilde{\mathcal{V}}^{\mathcal{R}}$ and the physical mass $m_{\tilde{\nu}^{\mathcal{R}}}$ can be expressed as $\tilde{\mathcal{V}}^{\mathcal{I}}$ and $m_{\tilde{\nu}^{\mathcal{I}}}$, respectively in the rest of the paper. With respect to charged sleptons, the LH sector element is given by $m_{\tilde{L}'}^2 + m_l^2 - m_D m_D^T - m_W^2 \cos 2\beta$.

Afterwards we discuss the last term of the superpotential. For the superpotential term $\lambda'_{ijk} \hat{L}_i \hat{Q}_j \hat{D}_k$, the corresponding Lagrangian in the flavour basis is obtained as

$$\begin{aligned} \mathcal{L}_{\text{LQD}} = & \lambda'_{ijk} (\tilde{\nu}_{Li} \bar{d}_{Rk} d_{Lj} + \tilde{d}_{Lj} \bar{d}_{Rk} \nu_{Li} + \tilde{d}_{Rk}^* \bar{\nu}_{Li}^c d_{Lj} \\ & - \tilde{l}_{Li} \bar{d}_{Rk} u_{Lj} - \tilde{u}_{Lj} \bar{d}_{Rk} l_{Li} - \tilde{d}_{Rk}^* \bar{l}_{Li}^c u_{Lj}) + \text{h.c.}, \end{aligned} \quad (2.8)$$

where “ c ” indicates the charge conjugated fermions. Then in the context of mass eigenstates for the down quarks and charged leptons, the Lagrangian above with other fields $\tilde{\nu}_L$, ν_L and u_L (aligned with \tilde{u}_L) rotated to mass eigenstates by mixing matrices $\tilde{\mathcal{V}}^{\mathcal{I}(\mathcal{R})}$, \mathcal{V} and K respectively, is given by

$$\begin{aligned} \mathcal{L}'_{\text{LQD}} = & \lambda_{ijk}^{\mathcal{I}(\mathcal{R})} \tilde{\nu}_v \bar{d}_{Rk} d_{Lj} + \lambda_{ijk}^{\mathcal{N}} (\tilde{d}_{Lj} \bar{d}_{Rk} \nu_v + \tilde{d}_{Rk}^* \bar{\nu}_v^c d_{Lj}) \\ & - \tilde{\lambda}'_{ilk} (\tilde{l}_{Li} \bar{d}_{Rk} u_{Ll} + \tilde{u}_{Ll} \bar{d}_{Rk} l_{Li} + \tilde{d}_{Rk}^* \bar{l}_{Li}^c u_{Ll}) + \text{h.c.}, \end{aligned} \quad (2.9)$$

where all the fields are represented by the mass eigenstates. Concretely, ν_v and $\tilde{\nu}_v$ are in the mass eigenstate with the index $v = 1, 2, \dots, 9$ and the three neo- λ' terms are deduced as $\lambda_{ijk}^{\mathcal{I}(\mathcal{R})} = \lambda'_{ijk} \tilde{\mathcal{V}}_{vi}^{\mathcal{I}(\mathcal{R})*}$, $\lambda_{ijk}^{\mathcal{N}} = \lambda'_{ijk} \mathcal{V}_{vi}^*$ and $\tilde{\lambda}'_{ilk} = \lambda'_{ijk} K_{lj}^*$. In the following, we call the diagrams including these λ' couplings by “ λ' diagrams”, otherwise by “non- λ' diagrams”.

By the end of this section, we should mention the chargino and neutralino mass matrices

in the MSSM sector of this model. The chargino mass matrix is [171]

$$\mathcal{M}_{\chi^\pm} = \begin{pmatrix} M_2 & \sqrt{2}m_w \sin \beta \\ \sqrt{2}m_w \cos \beta & \mu \end{pmatrix}, \quad (2.10)$$

where the parameter M_2 is the wino mass and μ is related to the Higgsino mass. The mixing matrices V and U diagonalize \mathcal{M}_{χ^\pm} by $U^* \mathcal{M}_{\chi^\pm} V^\dagger = \mathcal{M}_{\chi^\pm}^{\text{diag}}$. As to the neutralino mass matrix \mathcal{M}_{χ^0} in the basis $(\tilde{B}, \tilde{W}^3, \tilde{H}_d^0, \tilde{H}_u^0)^T$ [171],

$$\mathcal{M}_{\chi^0} = \begin{pmatrix} M_1 & 0 & -\frac{ev_d}{2 \cos \theta_W} & \frac{ev_u}{2 \cos \theta_W} \\ 0 & M_2 & \frac{ev_d}{2 \sin \theta_W} & -\frac{ev_u}{2 \sin \theta_W} \\ -\frac{ev_d}{2 \cos \theta_W} & \frac{ev_d}{2 \sin \theta_W} & 0 & -\mu \\ \frac{ev_u}{2 \cos \theta_W} & -\frac{ev_u}{2 \sin \theta_W} & -\mu & 0 \end{pmatrix}, \quad (2.11)$$

with M_1 being the bino mass and θ_W being the weak mixing angle, it is diagonalized by $N \mathcal{M}_{\chi^0} N^T = \mathcal{M}_{\chi^0}^{\text{diag}}$.

3 $b \rightarrow s \ell^+ \ell^-$ process in RPV-MSSMIS

In RPV-MSSMIS, the tree-level diagram of the $b \rightarrow s \ell^+ \ell^-$ process which exchanges \tilde{u}_L makes the RH-quark-vector-current contribution

$$C'_{9,\mu} = -C'_{10,\mu} = -\frac{\sqrt{2}\pi^2}{G_F \eta_t e^2} \frac{\tilde{\lambda}'_{2i2} \tilde{\lambda}_{2i3}^{\prime*}}{m_{\tilde{u}_L}^2}, \quad (3.1)$$

where the related operator $\mathcal{O}'_{9(10)}$ is given by P_L changed into P_R in $\mathcal{O}_{9(10)}$. This contribution is unwanted to explain $b \rightarrow s \ell^+ \ell^-$ anomalies. Besides, the box diagrams of the $b \rightarrow s \ell^+ \ell^-$ process also give such RH-quark-vector-current contributions which engage the sneutrino $\tilde{\nu}_{\nu(\prime)}$ and LH slepton $\tilde{l}_{L\ell}$ with the coupling factors $\lambda_{vi2}^{\mathcal{I}} \lambda_{v'i3}^{\mathcal{I}*}$ and $\tilde{\lambda}'_{\ell i2} \tilde{\lambda}_{\ell i3}^{\prime*}$, respectively (see Eq. (A.2) and Eq. (A.7)). We concentrate on the loop effects of sneutrinos which are not expected heavy decoupled, and furthermore, the NP particles engaged in $b \rightarrow s \ell^+ \ell^-$ and other related processes such as $B \rightarrow X_s \gamma$, $B_s - \bar{B}_s$ mixing, etc., are expected to have masses as sub-TeV or TeV scale, except for the heavy decoupled particles. Thus, we set the λ' couplings taken at 0.5 TeV scale called the μ_{NP} scale and assume λ'_{ijk} non-negligible with the single value k at this scale. It is called the single value k assumption in this work, and the index k is not be summed over in

equations from here on. This kind of assumption is also taken in recent works for the similar phenomenological consideration, such as Refs. [43–47]. Authors of Ref. [45] further assume that $\lambda'_{ij1} = \lambda'_{ij2} = 0$ which are adopted in Refs. [46, 47] considering the bounds of $\tau \rightarrow \mu \rho^0$ and $\tau \rightarrow \mu \phi$ decays, while these constraints can also be negligible by setting sufficiently heavy $m_{\tilde{u}_{Lj}}$.

We scrutinize all the one-loop Feynman diagrams of $b \rightarrow s \ell^+ \ell^-$ process in RPV-MSSMIS under the single value k assumption. For the box diagrams, there are eleven chargino box diagrams including nine λ' diagrams (figure 1a) and two non- λ' diagrams (figure 1b), fourteen W with W Goldstones or charged Higgs box (called W/H^\pm box here) diagrams including ten λ' ones (figure 1c) and four non- λ' ones (figure 1d), and three $4\lambda'$ box diagrams (figure 1e and f). The whole contributions of box diagrams are listed in the appendix (see formulas of the Passarino–Veltman functions D_2 and D_0 in Ref. [47], where $D_{2(0)}[m_1^2, m_2^2, m_3^2, m_4^2]$ is denoted as $D_{2(0)}[m_1, m_2, m_3, m_4]$ in this paper, respectively). The Wilson coefficients in the appendix are given at μ_{NP} , and if we consider the single value k assumption, only the LH-quark-vector-current contributions, $C_{9(10)}^{\text{NP}}(\mu_{\text{NP}})$ are existent and all the RH-quark-vector-current ones, $C_{9(10)}^{\text{NP}}(\mu_{\text{NP}})$ vanish. Then the Wilson coefficients run down to the scale of $\mu_b = m_b$ under QCD renormalization. One can find that $C_{9(10)}^{\text{NP}}(\mu_b) \approx C_{9(10)}^{\text{NP}}(\mu_{\text{NP}})$ [189] and $C_{9(10)}^{\text{NP}}(\mu_b)$ vanishes due to the approximate conservation of (axial-)vector currents. Thus we can constrain the model parameters related to $C_{9(10)}(\mu_b)$ using the global fit results introduced in section 1.

From the appendix, one can see that \tilde{l}_i and \tilde{d}_{Lj} in the box diagrams can be forbidden under the assumption of a single value k . In the following we further assume that $m_{\tilde{d}_{Rk}}$ is sufficiently heavy to focus on the contributions of sneutrinos as the bridge between the trilinear RPV term and the inverse seesaw mechanism. Therefore, contributions including \tilde{d}_{Rk} are negligible and can be removed. Besides, we also set $m_{\tilde{u}_{Lj}}$ adequately heavy³. Because the LFU violating contributions mainly from $\mu^+ \mu^-$ channel are expected to explain $b \rightarrow s \ell^+ \ell^-$ anomalies in both scenario A and B, we will set that $\mathcal{M}_{\nu^{\mathcal{I}(\mathcal{R})}}^2$ has no flavour mixing and the electron-flavour elements with both LH and RH chirality are sufficiently heavy. Then nearly all box contributions to $b \rightarrow s e^+ e^-$ transition and some box contributions to $b \rightarrow s \mu^+ \mu^-$ transition can be eliminated and afterwards we show which contributions remain.

Firstly among these non-negligible chargino box diagrams, the non- λ' diagram with RH sneutrinos previously discussed in Ref. [56] is recalculated by us. We find the Wilson coefficient C_9^{NP} from this diagram equals to $-C_{10}^{\text{NP}}$, which is different from the condition that $C_9^{\text{NP}} = C_{10}^{\text{NP}}$

³In this work, $m_{\tilde{d}_{Rk}}$ and $m_{\tilde{u}_{Lj}}$ are set as around 10 TeV.

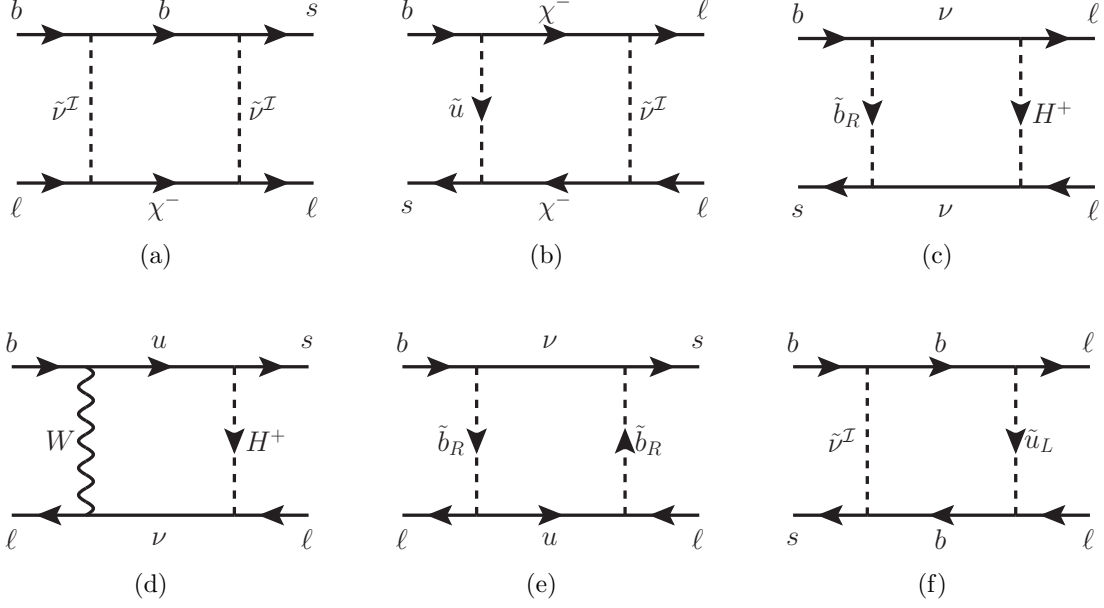


Figure 1: Box diagrams for $b \rightarrow s \ell^+ \ell^-$ process in our parameter scheme. Figures 1(a) and 1(b) show an example of λ' diagrams and non- λ' diagrams within chargino boxes, respectively. Figures 1(c) and 1(d) show an example of λ' diagrams and non- λ' diagrams within W/H^\pm box, respectively. Figures 1(e) and 1(f) show the three $4\lambda'$ box diagrams with the $\tilde{\nu}^{\mathcal{R}}$ -engaged diagram omitted.

in Ref. [56]. The related C_9^{NP} , namely as $C_V^{\chi^\pm(1)}$ in this paper, is given by

$$C_V^{\chi^\pm(1)} = -\frac{\sqrt{2}\pi^2 i}{2G_F \eta_t e^2} y_{u_i}^2 K_{i3} K_{i2}^* V_{m2}^* V_{n2} (g_2 V_{m1} \tilde{\mathcal{Y}}_{v2}^{\mathcal{I}} - V_{m2} Y_{2v}^{\mathcal{I}}) \\ (g_2 V_{n1}^* \tilde{\mathcal{Y}}_{v2}^{\mathcal{I}} - V_{n2}^* Y_{2v}^{\mathcal{I}}) D_2[m_{\tilde{\nu}_v^{\mathcal{I}}}, m_{\chi_m^\pm}, m_{\chi_n^\pm}, m_{\tilde{u}_{Ri}}], \quad (3.2)$$

where the Yukawa couplings $y_{u_i} = \sqrt{2}m_{u_i}/v_u$ and $Y_{\ell v}^{\mathcal{I}} = (Y_\nu)_{j\ell} \tilde{\mathcal{Y}}_{v(j+3)}^{\mathcal{I}*}$. This formula can be seen in the second term of Eq (A.1).

Then we show the λ' within chargino box diagram containing the RPV interactions between singlet sneutrinos and quarks. The contribution is given by

$$C_V^{\chi^\pm(2)} = \frac{\sqrt{2}\pi^2 i}{2G_F \eta_t e^2} \lambda_{v3k}^{\mathcal{I}} \lambda_{v'2k}^{\mathcal{I}*} (g_2 V_{m1}^* \tilde{\mathcal{Y}}_{v2}^{\mathcal{I}} - V_{m2}^* Y_{2v}^{\mathcal{I}}) \\ (g_2 V_{m1} \tilde{\mathcal{Y}}_{v'2}^{\mathcal{I}} - V_{m2} Y_{2v'}^{\mathcal{I}}) D_2[m_{\tilde{\nu}_v^{\mathcal{I}}}, m_{\tilde{\nu}_{v'}^{\mathcal{I}}}, m_{\chi_m^\pm}, m_{d_k}], \quad (3.3)$$

which appears in the third term of Eq (A.1).

The non-ignorable W/H^\pm box contributions in Eq. (A.3) are

$$\begin{aligned}
C_{9,\ell}^{W/H^\pm(1)} = -C_{10,\ell}^{W/H^\pm(1)} = & -\frac{\sqrt{2}\pi^2 i}{2G_F\eta_t e^2} \left(y_{u_i}^2 K_{i3} K_{i2}^* Z_{H_{h2}}^2 Z_{H_{h'2}}^2 |Y_{\ell v}^{\mathcal{N}}|^2 D_2[m_{\nu_v}, m_{u_i}, m_{H_h}, m_{H_{h'}}] \right. \\
& - 4g_2^2 m_{u_i} y_{u_i} m_{\nu_v} K_{i3} K_{i2}^* Z_{H_{h2}}^2 \text{Re}(\mathcal{V}_{v\ell} Y_{\ell v}^{\mathcal{N}*}) D_0[m_{\nu_v}, m_{u_i}, m_W, m_{H_h}] \\
& \left. + 5g_2^4 K_{i3} K_{i2}^* |\mathcal{V}_{v\ell}|^2 D_2[m_{\nu_v}, m_{u_i}, m_W, m_W] \right), \tag{3.4}
\end{aligned}$$

where the mixing matrix elements $Z_{H_{12}} = -\sin\beta$, $Z_{H_{22}} = -\cos\beta$ with Goldstone mass $m_{H_1} = m_W$ and charged Higgs mass $m_{H_2} = m_{H^\pm}$ and $Y_{\ell v}^{\mathcal{N}} = (Y_\nu)_{j\ell} \mathcal{V}_{v(j+3)}^*$. It is obvious that these W/H^\pm box contributions include SM effects, which cannot be separated naively from NP effects because of the generation and the chiral mixing of massive neutrinos. In addition, these contributions still contain both the $\mu^+\mu^-$ channel sector and e^+e^- channel sector. We will further investigate these contributions in detail at section 5.

Next we show the penguin contributions. Indeed, the Wilson coefficients of Z -boson penguin diagrams are negligible. While the contributions of photon penguin diagrams can be non-ignorable, where the λ' diagrams (figure 2a) give

$$C_U^{\gamma(1)} = -\frac{\sqrt{2}\lambda_{v33}^{\mathcal{I}}\lambda_{v23}^{\mathcal{I}*}}{36G_F\eta_t m_{\tilde{\nu}_v^{\mathcal{I}}}^2} \left(\frac{4}{3} + \log \frac{m_b^2}{m_{\tilde{\nu}_v^{\mathcal{I}}}^2} \right), \tag{3.5}$$

for the case of $k = 3$ and the non- λ' contributions (figure 2b and c) namely as $C_U^{\gamma(2)}$ are also calculated by us for completeness.

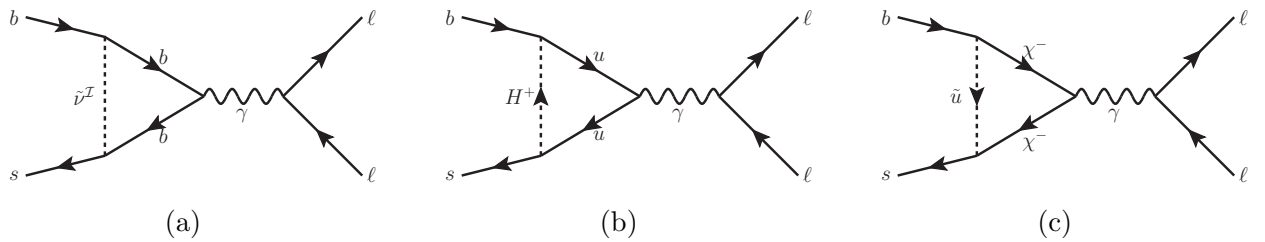


Figure 2: Photon penguin diagrams for $b \rightarrow s\ell^+\ell^-$ process in our parameter scheme. Here each example of the λ' diagrams (left) and the non- λ' diagrams with W/H^\pm (middle) and charginos (right) engaged are shown respectively.

4 The $(g-2)_\ell$ and other constraints

In this section, we introduce the NP contributions to $(g-2)_\ell$ and other related processes.

4.1 The muon (electron) anomalous magnetic moment

The amplitude of the $\ell \rightarrow \ell \gamma$ ($\ell = e, \mu$) transition is given by

$$i\mathcal{M} = ie\bar{\ell} \left(\gamma^\eta + a_\ell \frac{i\sigma^{\eta\beta} q_\beta}{2m_\ell} \right) \ell A_\eta \quad (4.1)$$

in the zero limit of photon moment q . The second term in the bracket gives the loop corrections and a_ℓ is called the anomalous magnetic moment for the related lepton.

The SM-like diagrams that only involve SM particles give the same contributions to a_ℓ as the SM. Hence the SUSY part can contribute to the observed anomaly Δa_ℓ [141]. The one-loop chargino and neutralino contributions in RPV-MSSMIS are given here, with referring to Refs. [122, 128, 141, 190],

$$\begin{aligned} \delta a_\ell^{\chi^\pm} &= \frac{m_\ell}{16\pi^2} \left[\frac{m_\ell}{6m_{\tilde{\nu}_v}^2} (|c_{mv}^{\ell L}|^2 + |c_{mv}^{\ell R}|^2) F_1^C(m_{\chi_m^\pm}^2/m_{\tilde{\nu}_v}^2) + \frac{m_{\chi_m^\pm}}{m_{\tilde{\nu}_v}^2} \text{Re}(c_{mv}^{\ell L} c_{mv}^{\ell R}) F_2^C(m_{\chi_m^\pm}^2/m_{\tilde{\nu}_v}^2) \right], \\ \delta a_\ell^{\chi^0} &= \frac{m_\ell}{16\pi^2} \left[-\frac{m_\ell}{6m_{\tilde{l}_i}^2} (|n_{ni}^{\ell L}|^2 + |n_{ni}^{\ell R}|^2) F_1^N(m_{\chi_n^0}^2/m_{\tilde{l}_i}^2) + \frac{m_{\chi_n^0}}{m_{\tilde{l}_i}^2} \text{Re}(n_{ni}^{\ell L} n_{ni}^{\ell R}) F_2^N(m_{\chi_n^0}^2/m_{\tilde{l}_i}^2) \right], \end{aligned} \quad (4.2)$$

where

$$\begin{aligned} c_{mv}^{\ell R} &= y_\ell U_{m2} \tilde{\mathcal{V}}_{v\ell}^{\mathcal{I}}, \quad c_{mv}^{\ell L} = -g_2 V_{m1} \tilde{\mathcal{V}}_{v\ell}^{\mathcal{I}} + V_{m2} Y_{\ell v}^{\mathcal{I}}; \\ n_{ni}^{\ell R} &= \sqrt{2} g_1 N_{n1} \delta_{i(\ell+3)} + y_\ell N_{n3} \delta_{i\ell}, \quad n_{ni}^{\ell L} = \frac{1}{\sqrt{2}} (g_2 N_{n2} + g_1 N_{n1}) \delta_{i\ell} - y_\ell N_{n3} \delta_{i(\ell+3)}, \end{aligned} \quad (4.3)$$

and functions

$$\begin{aligned} F_1^C(x) &= \frac{1}{(1-x)^4} (2 + 3x - 6x^2 + x^3 + 6x \log x), \\ F_2^C(x) &= -\frac{1}{(1-x)^3} (3 - 4x + x^2 + 2 \log x), \\ F_1^N(x) &= \frac{1}{(1-x)^4} (1 - 6x + 3x^2 + 2x^3 - 6x^2 \log x), \\ F_2^N(x) &= \frac{1}{(1-x)^3} (1 - x^2 + 2x \log x). \end{aligned} \quad (4.4)$$

The flavour mixing of RH sleptons is not considered here, and neither is the flavour mixing of LH sleptons. Since the contributions from λ' diagrams are negligible for the heavy \tilde{b}_R and \tilde{u}_L , they are not shown in Eq. (4.3). The difference from MSSM is the form factor $c_{mv}^{\ell L}$ in Eq. (4.3), where the extra $V_{m2} Y_{\ell v}^{\mathcal{I}}$ term can make an enhancement. Because the measured Δa_e

has different features compared with Δa_μ , we consider the scheme of $|\delta a_\mu^{\chi^\pm}| \gg |\delta a_e^{\chi^\pm}| \approx 0$ and $|\delta a_e^{\chi^0}| \gg |\delta a_\mu^{\chi^0}| \approx 0$ [131]. And thus, the muon generation associated with RH sleptons is set sufficiently heavy as well as heavy \tilde{L}'_1 which is already assumed in section 3. Afterwards we expect $1.92(1.33) \leq |\delta a_\mu^{\chi^\pm} + \delta a_\mu^{\chi^0}| \times 10^9 \leq 3.10(3.69)$ to be in accord with a_μ data at $1(2)\sigma$ respectively.

4.2 Tree-level processes

In the following we investigate related transition bounds which exchange \tilde{d}_{Rk} at the tree level. On account of the assumption of heavy $m_{\tilde{d}_{Rk}} \sim 10$ TeV, the neutral current processes $B \rightarrow K^{(*)}\nu\bar{\nu}$, $B \rightarrow \pi\nu\bar{\nu}$, $D^0 \rightarrow \mu^+\mu^-$ as well as the charged current processes $B \rightarrow \tau\nu$, $D_s \rightarrow \tau\nu$ and $\tau \rightarrow K\nu$ provide no effective constraints. Besides, there are some tree-level processes which may make some slight bounds to mention here.

The SM prediction $\mathcal{B}(K^+ \rightarrow \pi^+\nu\bar{\nu})_{\text{SM}} = (9.24 \pm 0.83) \times 10^{-11}$ [191] combined with the experimental measurement $\mathcal{B}(K^+ \rightarrow \pi^+\nu\bar{\nu})_{\text{exp}} = (1.7 \pm 1.1) \times 10^{-10}$ [192] induces the constraint. The effective Lagrangian for $K \rightarrow \pi\nu\bar{\nu}$ decay can be described by

$$\mathcal{L}_{\text{eff}} = (C^{\text{SM}}\delta_{ii'} + C_{ii'}^{\text{NP}})(\bar{d}\gamma_\mu P_L s)(\bar{\nu}_i\gamma^\mu P_L \nu_{i'}) + \text{h.c.}, \quad (4.5)$$

where the SM contributes $C^{\text{SM}} = -\frac{\sqrt{2}G_F e^2 K_{ts} K_{td}^*}{4\pi^2 \sin^2 \theta_W} X(x_t)$ and $X(x_t) = \frac{x_t(x_t+2)}{8(x_t-1)} + \frac{3x_t(x_t-2)}{8(x_t-1)^2} \log(x_t)$ with $x_t = m_t^2/m_W^2$ [193]. While the NP contribution is

$$C_{ii'}^{\text{NP}} = \frac{\lambda_{i'2k}^{\mathcal{N}} \lambda_{i1k}^{\mathcal{N}*}}{2m_{\tilde{d}_{Rk}}^2}. \quad (4.6)$$

Then the bound is obtained as $|\lambda_{i'2k}^{\mathcal{N}} \lambda_{i1k}^{\mathcal{N}*}| < 0.074$ when $m_{\tilde{d}_{Rk}}$ around 10 TeV [47], and hence, we can set $|\lambda_{i1k}^{\mathcal{N}}| \lesssim 10^{-2}$ to avoid this bound.

As to the processes of τ decaying to a μ and a vector meson, $\tau \rightarrow \mu\rho^0$ and $\tau \rightarrow \mu\phi$, the branching fraction is given by [194],

$$\mathcal{B}(\tau \rightarrow \mu V) = \frac{\tau_\tau f_V^2 m_\tau^3}{128\pi} |A_V|^2 \left(1 - \frac{m_V^2}{m_\tau^2}\right) \left(1 + \frac{m_V^2}{m_\tau^2} - 2\frac{m_V^4}{m_\tau^4}\right), \quad (4.7)$$

where V stands for ρ^0 and ϕ . The mean lifetime of tauon $\tau_\tau = 290.3 \pm 0.5$ fs [192] and the decay constants f_V have the value of $f_{\rho^0} = 153$ MeV and $f_\phi = 237$ MeV respectively [45]. And

A_V is given by [194]

$$\begin{aligned} A_{\rho^0} &= \frac{\tilde{\lambda}'_{3j1}\tilde{\lambda}'_{2j1}}{2m_{\tilde{u}_{Lj}}^2} - \frac{\tilde{\lambda}'_{31k}\tilde{\lambda}'_{21k}}{2m_{\tilde{d}_{Rk}}^2}, \\ A_\phi &= \frac{\tilde{\lambda}'_{3j2}\tilde{\lambda}'_{2j2}}{2m_{\tilde{u}_{Lj}}^2}. \end{aligned} \quad (4.8)$$

The most recent experimental upper limits on the branch fractions of the two processes at 90% confidence level (CL) are $\mathcal{B}(\tau \rightarrow \mu\rho^0) < 1.2 \times 10^{-8}$ and $\mathcal{B}(\tau \rightarrow \mu\phi) < 8.4 \times 10^{-8}$ [192]. We can obtain the bounds [45]

$$\begin{aligned} |\tilde{\lambda}'_{3j1}\tilde{\lambda}'_{2j1} - \tilde{\lambda}'_{31k}\tilde{\lambda}'_{21k}| &< 1.9, \\ |\tilde{\lambda}'_{3j2}\tilde{\lambda}'_{2j2}| &< 3.6, \end{aligned} \quad (4.9)$$

respectively when both $m_{\tilde{d}_{Rk}}$ and $m_{\tilde{u}_{Lj}}$ around 10 TeV. Under the negligible $|\lambda'_{i1k}|$ assumption, the bounds of Eq. (4.9) turn into $|\tilde{\lambda}'_{321}\tilde{\lambda}'_{221} + \tilde{\lambda}'_{331}\tilde{\lambda}'_{231}| < 1.9$ or $|\tilde{\lambda}'_{322}\tilde{\lambda}'_{222} + \tilde{\lambda}'_{332}\tilde{\lambda}'_{232}| < 3.6$ when the single value k is restricted to 1 or 2 for the nonzero λ'_{ijk} , respectively. While there exists no effective bound when k is restricted to 3. We can see that if k is restricted to 1(2) for the nonzero λ'_{ijk} , $|\lambda'_{ij1(2)}|$ should be below around 1(1.3), respectively, in the case of no cancelling out.

4.3 $B \rightarrow X_s\gamma$

At one-loop level, the photon penguin diagrams in figure 2 also contribute to the electromagnetic dipole operator $\mathcal{O}_7 = \frac{m_b}{e}(\bar{s}\sigma^{\mu\nu}P_R b)F_{\mu\nu}$ constrained by the $B \rightarrow X_s\gamma$ decay. The NP Wilson coefficient C_7^{NP} includes charged Higgs contributions and the effects from the chargino with \tilde{u}_{Rj} as well as the RPV contributions engaging sneutrinos.

The RPV contribution is given by

$$C_7^{\text{RPV}} = \frac{\sqrt{2}\lambda'_{v3k}\lambda'_{v2k}}{144G_F\eta_t m_{\tilde{\nu}_v^I}^2}. \quad (4.10)$$

Compared with $C_U^{\gamma(1)}$ in Eq. (3.5), C_7^{RPV} contains the common part $\lambda'_{v3k}\lambda'_{v2k}/m_{\tilde{\nu}_v^I}^2$ while no logarithmic term.

The contribution of charged Higgs is given by

$$C_7^{H^\pm} = \frac{1}{3 \tan^2 \beta} F_7^{(1)}(y_t) + F_7^{(2)}(y_t), \quad (4.11)$$

where the form factors are $F_7^{(1)}(y_t) = \frac{y_t(7-5y_t-8y_t^2)}{24(y_t-1)^3} + \frac{y_t^2(3y_t-2)}{4(y_t-1)^4} \log y_t$ and $F_7^{(2)}(y_t) = \frac{y_t(3-5y_t)}{12(y_t-1)^2} + \frac{y_t(3y_t-2)}{6(y_t-1)^3} \log y_t$ with $y_t = m_t^2/m_{H^\pm}^2$. One can see the $F_7^{(2)}(y_t)$ part is not suppressed when $\tan \beta$ is large and this is unlike the H^\pm contributions to $C_{9(10)}$ which are entirely suppressed by large $\tan \beta$. The formulas of $C_7^{\chi^\pm}$ engaging the chargino together with \tilde{u}_{Rj} and the QCD corrections can be seen in Ref [195].

The recent measurements of branching ratio $\mathcal{B}(B \rightarrow X_s \gamma)_{\text{exp}} \times 10^4 = 3.43 \pm 0.21 \pm 0.07$ [89] is consist with the SM prediction $\mathcal{B}(B \rightarrow X_s \gamma)_{\text{SM}} \times 10^4 = 3.36 \pm 0.23$ [196] and induce the bound to $|C_7^{\text{NP}}| < 0.025$ [48].

4.4 $B_s - \bar{B}_s$ mixing

Another process we should consider is $B_s - \bar{B}_s$ mixing, mastered by the Lagrangian

$$\mathcal{L}_{\text{eff}} = (C_{B_s}^{\text{SM}} + C_{B_s}^{\text{NP}})(\bar{s}\gamma_\mu P_L b)(\bar{s}\gamma^\mu P_L b) + \text{h.c.}, \quad (4.12)$$

where the non-negligible NP contribution is given by

$$C_{B_s}^{\text{NP}} = -\frac{i}{8} \left(\lambda_{v3k}^{\mathcal{I}} \lambda_{v2k}^{\mathcal{I}*} \lambda_{v'3k}^{\mathcal{I}} \lambda_{v'2k}^{\mathcal{I}*} D_2[m_{\tilde{\nu}_v^{\mathcal{I}}}, m_{\tilde{\nu}_{v'}^{\mathcal{I}}}, m_{d_k}, m_{d_k}] \right. \\ \left. + y_{u_i}^2 y_{u_j}^2 (K_{i3} K_{i2}^*)(K_{j3} K_{j2}^*) |V_{m2} V_{n2}|^2 D_2[m_{\chi_m^\pm}, m_{\chi_n^\pm}, m_{\tilde{u}_{Ri}}, m_{\tilde{u}_{Rj}}] \right) \quad (4.13)$$

including the λ' diagram with double sneutrinos and the non- λ' diagram with double RH su-quarks, and the SM contribution $C_{B_s}^{\text{SM}} = -\frac{1}{4\pi^2} G_F^2 m_W^2 \eta_t^2 S(x_t)$ with the function $S(x_t) = \frac{x_t(4-11x_t+x_t^2)}{4(x_t-1)^2} + \frac{3x_t^3 \log(x_t)}{2(x_t-1)^3}$. With the measurement of $\Delta M_s^{\text{exp}} = (17.757 \pm 0.021) \text{ ps}^{-1}$ [89]⁴, the recent SM prediction $\Delta M_s^{\text{SM}} = (18.4_{-1.2}^{+0.7}) \text{ ps}^{-1} = (1.04_{-0.07}^{+0.04}) \Delta M_s^{\text{exp}}$ [198] leads to the bound of

$$0.90 < |1 + C_{B_s}^{\text{NP}}/C_{B_s}^{\text{SM}}| < 1.11, \quad (4.14)$$

at 2σ level.

⁴The newly updated experimental result of ΔM_s by LHCb has been reported [197]. The combined result with previous LHCb measurements gives $\Delta M_s^{\text{LHCb}} = (17.7656 \pm 0.0057) \text{ ps}^{-1}$ with the improved precision. Using this new combined result will not change the Eq. (4.14).

4.5 Lepton flavour violating decays

We discuss the lepton flavour violating decays including $\tau \rightarrow \ell\gamma$, $\mu \rightarrow e\gamma$, $\tau \rightarrow \ell\ell\ell$, $\mu \rightarrow eee$ and $\tau \rightarrow \ell'\ell\ell$. Firstly, the λ' -diagram contributions can be eliminated when \tilde{b}_R is sufficiently heavy [47]. As to the non- λ' diagrams, all the neutralino-slepton diagrams contain flavour mixings of charged sleptons and all the chargino-sneutrino diagrams contain flavour mixings of sneutrinos (see Ref. [199] for concrete formulas). So the effects of these two kinds of diagrams vanish when there are no flavour mixing in the two mass matrices. For contributions of W/H^\pm -neutrino diagrams, they are always connected to these terms which are $\mathcal{V}_{(\alpha+3)v}^{T*}\mathcal{V}_{(\beta+3)v}^T$, $\mathcal{V}_{(\alpha+3)v}^{T*}\mathcal{V}_{\beta v}^T$ and $\mathcal{V}_{\alpha v}^{T*}\mathcal{V}_{\beta v}^T$ and their conjugate terms, where $\alpha, \beta = e, \mu, \tau$ and $\alpha \neq \beta$ [199]. In section 5.1, we will show all these terms contribute no effects under the particular structure of neutrino mass matrix. The same analyses can also be applied to the non- λ' diagrams in $B_s^0 \rightarrow \tau^\pm \mu^\mp$ and $B^+ \rightarrow K^+ \tau^\pm \mu^\mp$. For the λ' diagrams of these two processes, we refer to the detailed discussions in Ref. [46], and no obvious constraints are found.

4.6 Anomalous $t \rightarrow cV(h)$ decays

The SM predicts the branching ratios of $t \rightarrow cV$ decays (V stands for the vector bosons including Z , γ and the gluon g) and $t \rightarrow ch$ decay (h stands for SM-like Higgs) below the scale of $10^{-15} - 10^{-12}$ [200] due to the Glashow–Iliopoulos–Maiani suppression. This scale is beyond the detection capabilities at the collider in the near future. The most recent experimental 95% CL upper limits on the branching ratios of these top quark decays at the Large Hadron Collider (LHC) show that $\mathcal{B}(t \rightarrow cZ) < 2.4 \times 10^{-4}$ [201], $\mathcal{B}(t \rightarrow c\gamma) < 1.8 \times 10^{-4}$ [202], $\mathcal{B}(t \rightarrow cg) < 4.1 \times 10^{-4}$ [203] and $\mathcal{B}(t \rightarrow ch) < 1.1 \times 10^{-3}$ [204]. Compared with the effects from pure MSSM, the one-loop RPV diagrams can make more contributions [205, 206], and hence we will investigate these effects in our model.

For the $t \rightarrow cV$ decays, the effective tcV vertices are expressed as,

$$\begin{aligned} V^\mu(tcZ) &= ie \left(\gamma^\mu P_L A^Z + ik_\nu \sigma^{\mu\nu} P_R B^Z \right), \\ V^\mu(tc\gamma) &= ie \left(ik_\nu \sigma^{\mu\nu} P_R B^\gamma \right), \\ V^\mu(tcg) &= ig_s t^a \left(ik_\nu \sigma^{\mu\nu} P_R B^g \right), \end{aligned} \tag{4.15}$$

where k_ν is the momentum of the vector boson. The form factors A^Z and B^V are given by [205]

$$\begin{aligned}
A^Z &= \frac{\tilde{\lambda}_{i2k}'^* \tilde{\lambda}_{i3k}'}{16\pi^2} \left\{ f_1^Z B_1(m_t, m_{d_k}, m_{\tilde{l}_{Li}}) - f_2^Z [2c_{24} - \frac{1}{2} + m_Z^2(c_{12} + c_{23})](-p_t, p_c, m_{d_k}, m_{\tilde{l}_{Li}}, m_{d_k}) \right. \\
&\quad \left. - f_3^Z [2c_{24} + m_t^2(c_{11} - c_{12} + c_{21} - c_{23})](-p_t, k, m_{d_k}, m_{\tilde{l}_{Li}}, m_{\tilde{l}_{Li}}) \right\}, \\
B^V &= \frac{\tilde{\lambda}_{i2k}'^* \tilde{\lambda}_{i3k}'}{16\pi^2} \left\{ f_2^V m_t [c_{11} - c_{12} + c_{21} - c_{23}](-p_t, p_c, m_{d_k}, m_{\tilde{l}_{Li}}, m_{d_k}) \right. \\
&\quad \left. - f_3^V m_t [c_{11} - c_{12} + c_{21} - c_{23}](-p_t, k, m_{d_k}, m_{\tilde{l}_{Li}}, m_{\tilde{l}_{Li}}) \right\}, \tag{4.16}
\end{aligned}$$

where p_t and p_c are the momentums of top and charm quarks and functions B_1 and c_{ij} are the Passarino–Veltman integrals totally referring to Ref. [207]. The constants $f_1^Z = \frac{3-4\sin^2\theta_W}{6\sin\theta_W\cos\theta_W}$, $f_2^Z = -\frac{\sin\theta_W}{3\cos\theta_W}$ and $f_3^Z = \frac{2\sin^2\theta_W-1}{\sin\theta_W\cos\theta_W}$ are in the form factors A^Z and B^Z . And in B^γ , the relevant constants are $f_2^\gamma = 1/3$ and $f_3^\gamma = -1$. While $f_2^g = -1$ and $f_3^g = 0$ in B^g . Then the decay widths of $t \rightarrow cV$ are given

$$\begin{aligned}
\Gamma(t \rightarrow cZ)_{\text{NP}} &= \frac{e^2(m_t^2 - m_Z^2)^2}{32\pi m_t^3} \left[\left(2 + \frac{m_t^2}{m_Z^2}\right) |A^Z|^2 - 6m_t \text{Re}(A^Z B^{Z*}) + (2m_t^2 + m_Z^2) |B^Z|^2 \right], \\
\Gamma(t \rightarrow c\gamma)_{\text{NP}} &= \frac{e^2 m_t^3}{16\pi} |B^\gamma|^2, \\
\Gamma(t \rightarrow cg)_{\text{NP}} &= \frac{g_s^2 m_t^3}{12\pi} |B^g|^2. \tag{4.17}
\end{aligned}$$

As for the $t \rightarrow ch$ decay, the effective tch vertex is expressed as,

$$V(tch) = ie (P_L A_L^h + P_R A_R^h). \tag{4.18}$$

After omitting masses of charm quarks and all down-type quarks, one can obtain [206]

$$\begin{aligned}
A_R^h &= \frac{\tilde{\lambda}_{i2k}'^* \tilde{\lambda}_{i3k}'}{16\pi^2} \mathcal{Y}_{\tilde{l}_{Li}} m_t (c_{11} - c_{12}) (-p_t, k, 0, m_{\tilde{l}_{Li}}, m_{\tilde{l}_{Li}}), \\
A_L^h &= 0, \tag{4.19}
\end{aligned}$$

where factor $\mathcal{Y}_{\tilde{l}_{Li}} \approx \frac{m_Z}{\sin\theta_W\cos\theta_W} (\frac{1}{2} - \sin^2\theta_W) \cos 2\beta$ when the masses of leptons are omitted and the mass of CP -odd Higgs is sufficiently heavy. Then the decay width of $t \rightarrow ch$ is

$$\Gamma(t \rightarrow ch)_{\text{NP}} = \frac{e^2(m_t^2 - m_h^2)^2}{32\pi m_t^3} |A_R^h|^2. \tag{4.20}$$

The NP contributes to related branching ratios are given by $\mathcal{B}(t \rightarrow cV(h))_{\text{NP}} = \Gamma(t \rightarrow$

$cV(h))_{\text{NP}}/\Gamma(t \rightarrow bW)_{\text{SM}}$ where the dominant decay $t \rightarrow bW$ has the SM prediction $\Gamma(t \rightarrow bW)_{\text{SM}} = 1.42 \text{ GeV}$ [208].

4.7 LHC direct searches

The LHC direct searches have led to stringent limits on the masses of sbottoms and stops [209–215] and the recent searches [213–215] have excluded the heavy stops more than 1.35 TeV. In view of that \tilde{d}_{Rk} and \tilde{u}_{Li} have already been set adequately heavy, we further set $m_{\tilde{u}_{Ri}} > 1.4 \text{ TeV}$.

For the constraints on LH sleptons as mentioned in section 2, when considering non-zero λ couplings, the lower bounds of $m_{\tilde{\nu}_L}$ and $m_{\tilde{l}}$ reach TeV scale [182–184]. Because only non-zero λ' couplings are restricted in this work, LH sleptons decaying to pure leptons directly is secondary and processes without λ interactions should be taken into consideration mainly. We consider the searches which focus on LH sleptons decaying into leptons and the lightest neutralino χ_1^0 [216–218], and the recent ATLAS results [217] show that the LH sleptons which are heavier than χ_1^0 can avoid the exclusion for $m_{\chi_1^0} \gtrsim 300 \text{ GeV}$. Besides, the compressed scenario that the lightest chargino mass $m_{\chi_1^\pm}$ is slightly heavier than $m_{\chi_1^0}$ [219], is adopted. Thus we will let inputs inducing $m_{\chi_1^\pm} \gtrsim m_{\chi_1^0} \gtrsim 300 \text{ GeV}$ and $m_{\tilde{l}_L} > 300 \text{ GeV}$.

5 Numerical results and discussions

In this section, we investigate $b \rightarrow s\ell^+\ell^-$ anomalies numerically as well as the a_μ anomaly and the related constraints.

5.1 Choice of input parameters

First parts of input parameters used throughout the paper are collected in table 1, which includes the lepton oscillation data [74] under the normal ordering (NO) assumption of LH neutrino masses. In addition, we further keep $\delta_{\text{CP}} = \pi$ to omit the CP violation in U^{PMNS} . The lightest neutrino mass is set zero to have the masses of three-flavour light neutrinos as $\{0, 0.008, 0.05\} \text{ eV}$ with $m_\nu^{\text{diag}} \approx \text{diag}(0, \sqrt{\Delta m_{21}^2}, \sqrt{\Delta m_{31}^2})$ [222]. Then we collect the fixed values of relevant model parameters in table 2. The sets give $m_{\chi_1^\pm} = 325 \text{ GeV}$ and $m_{\chi_1^0} = 307 \text{ GeV}$ which are in accord with the constraints discussed in section 4.7. Besides, we set the diagonal parameters for Y_ν , M_R , $m_{\tilde{L}'}$, $m_{\tilde{R}}$, B_{M_R} and A_ν in Eq. (2.7) so that the sneutrino

QCD and EW parameters [192]					
$G_F[10^{-5} \text{ GeV}^{-2}]$	$\alpha_e(m_Z)$	$\alpha_s(m_Z)$	$m_W[\text{GeV}]$	$\sin^2 \theta_W$	
1.1663787	1/128	0.1179(10)	80.379	0.2312	
Quark and lepton masses [GeV] [192]					
$\overline{m}_b(\overline{m}_b)$	$\overline{m}_c(\overline{m}_c)$	m_t	m_e	m_μ	m_τ
$4.18^{+0.03}_{-0.02}$	1.27(2)	172.76(30)	0.511×10^{-3}	0.1057	1.777
CKM Wolfenstein parameters [220]					
λ_{CKM}	A	$\bar{\rho}$	$\bar{\eta}$		
$0.22484^{+0.00025}_{-0.00006}$	$0.8235^{+0.0056}_{-0.0145}$	$0.1569^{+0.0102}_{-0.0061}$	$0.3499^{+0.0079}_{-0.0065}$		
Lepton oscillation parameters (NO) [74]					
$\sin^2 \theta_{12}$	$\sin^2 \theta_{23}$		$\sin^2 \theta_{13}$		
0.304(12)	$0.573^{+0.016}_{-0.020}$		$0.02219^{+0.00062}_{-0.00063}$		
$\delta_{\text{CP}}[^\circ]$	$\Delta m_{21}^2[10^{-5} \text{ eV}^2]$		$\Delta m_{31}^2[10^{-3} \text{ eV}^2]$		
197^{+27}_{-24}	$7.42^{+0.21}_{-0.20}$		$2.517^{+0.026}_{-0.028}$		

Table 1: Summary of parts of input parameters used throughout this paper.

Parameters	Sets	Parameters	Sets
$\tan \beta$	15	Y_ν	diag(0.7, 0.8, 0.5) [221]
M_1	320 GeV	M_R	diag(1, 1, 1) TeV
M_2	350 GeV	B_{M_R}	diag(0.5, 0.5, 0.5) TeV ²
μ	450 GeV	A_ν	0; diag(0, -1.5, 0) TeV
$m_{\tilde{u}_{Ri}}$	1.5 TeV	$m_{\tilde{L}'_1}$	5 TeV
$m_{\tilde{\mu}_R}$	5 TeV	$m_{\tilde{R}}$	diag(5, 0, 0) TeV

Table 2: The sets of fixed model parameters, defined at μ_{NP} scale. The two sets of A_ν are for scenario A and B respectively.

mixing matrices $\tilde{\mathcal{V}}^{\mathcal{I}(\mathcal{R})}$ only have chiral mixings without flavour mixings and let them have proper values to agree with the discussions in sections 3 and 4 ⁵. As for the remaining model parameters, $m_{\tilde{L}'_2}$, $m_{\tilde{L}'_3}$, λ'_{22k} , λ'_{23k} , λ'_{32k} and λ'_{33k} , they can vary freely in the ranges considered.

With related inputs in table 1 and table 2, the μ_S term in Eq. (2.4) can be figured out with m_D , M_R , U^{PMNS} and the light neutrino masses m_ν^{diag} through Eq. (2.5). Then we obtain the

⁵Under the premise of no flavour mixing in $\tilde{\mathcal{V}}^{\mathcal{I}(\mathcal{R})}$, we mention that sufficiently heavy $m_{\tilde{L}'_1}$ and $m_{\tilde{R}_1}$ can eliminate the box contributions to $b \rightarrow se^+e^-$ except for $C_{9,e}^{W/H^\pm(1)}$ in section 3; $m_{\tilde{\mu}_R}$ and $m_{\tilde{L}'_1}$ are set sufficiently heavy for the scheme of non-dominant $|\delta a_\mu^0|$ and $|\delta a_e^\pm|$ in section 4.1. The $\tilde{\mathcal{V}}^{\mathcal{I}(\mathcal{R})}$ without flavour mixings is also for satisfying the bounds from lepton flavour violating decays mentioned in section 4.5.

approximate numerical form of the mixing matrix \mathcal{V}^T ,

$$\mathcal{V}^T \approx \begin{pmatrix} 0.840 & 0.509 & -0.147 & -0.085i & 0 & 0 & 0.085 & 0 & 0 \\ -0.231 & 0.599 & 0.755 & 0 & 0.097i & 0 & 0 & 0.097 & 0 \\ 0.478 & -0.608 & 0.628 & 0 & 0 & 0.061i & 0 & 0 & -0.061 \\ 0 & 0 & 0 & 0.707i & 0 & 0 & 0.707 & 0 & 0 \\ 0 & 0 & 0 & 0 & -0.707i & 0 & 0 & 0.707 & 0 \\ 0 & 0 & 0 & 0 & 0 & -0.707i & 0 & 0 & -0.707 \\ -0.102 & -0.062 & 0.018 & -0.702i & 0 & 0 & 0.702 & 0 & 0 \\ 0.032 & -0.083 & -0.105 & 0 & 0.700i & 0 & 0 & 0.700 & 0 \\ -0.041 & 0.053 & -0.055 & 0 & 0 & 0.704i & 0 & 0 & -0.704 \end{pmatrix}, \quad (5.1)$$

corresponding to the light neutrino masses $m_{\nu_i} = \{0, 0.008, 0.05\}$ eV and the nearly degenerate heavy ones $m_{\nu_{v_h}}$ around 1 TeV. One can see that there is no flavour mixing when RH sector is engaged but chiral mixing exists. With the numerical result of Eq. (5.1), we can eliminate the $\mathcal{V}_{(\alpha+3)v}^{T*} \mathcal{V}_{(\beta+3)v}^T$ and $\mathcal{V}_{(\alpha+3)v}^{T*} \mathcal{V}_{\beta v}^T$ terms in the contributions of W/H^\pm -neutrino diagrams to the lepton flavour violating decays within section 4.5. $\mathcal{V}_{\alpha v}^{T*} \mathcal{V}_{\beta v}^T$ can be decomposed into the following two parts, $\sum_{v_h=4}^9 \mathcal{V}_{\alpha v_h}^{T*} \mathcal{V}_{\beta v_h}^T$ and $\sum_{i=1}^3 \mathcal{V}_{\alpha i}^{T*} \mathcal{V}_{\beta i}^T = -\sum_{v_h=4}^9 \mathcal{V}_{\alpha v_h}^{T*} \mathcal{V}_{\beta v_h}^T$ related to the nearly degenerate heavy neutrinos and light neutrinos respectively [188]. It can also be found that $\mathcal{V}_{\alpha v}^{T*} \mathcal{V}_{\beta v}^T$ provides no effects from Eq. (5.1). In sum, the lepton flavour violating decays mentioned in section 4.5 contribute no effective bounds in our input sets.

In the following we discuss the feature of $C_{9(10),\ell}^{W/H^\pm(1)}$ in Eq. (3.4) which includes the e^+e^- channel. The three terms of Eq. (3.4) contain $|\mathcal{V}_{(\ell+3)v}^T|^2$, $\text{Re}(\mathcal{V}_{\ell v}^T \mathcal{V}_{(\ell+3)v}^T)$ and $|\mathcal{V}_{\ell v}^T|^2$ respectively. For h or/and $h' = 2$ firstly, this part of Eq. (3.4) includes the contribution of charged Higgs and it can be ignored for the set of $\tan \beta = 15$. In the case of $h = h' = 1$, this part of Eq. (3.4) describes the contribution of seesaw-extended SM. $|\mathcal{V}_{\ell v}^T|^2$ in the third term is dominated by $|U_{\ell i}^{\text{PMNS}}|^2$, and thus, this term is nearly equal to the contribution of the original SM. Because $\text{Re}(\mathcal{V}_{\ell v}^T \mathcal{V}_{(\ell+3)v}^T)$ is negligible compared with $|\mathcal{V}_{(\ell+3)v}^T|^2$, we focus on the first term in Eq. (3.4) and the second term can be omitted safely. According to the discussion above, the pure NP

contribution $\Delta C_{9(10),\ell}^{W/H^\pm}$ in Eq. (3.4) is induced by only heavy neutrinos and is given by

$$\Delta C_{9,\ell}^{W/H^\pm} = \sum_{v_h=4}^9 -\frac{\sqrt{2}\pi^2 i}{2G_F\eta_t e^2} y_{u_i}^2 K_{i3} K_{i2}^* \sin^4 \beta |Y_{\nu\ell} \mathcal{V}_{(\ell+3)v_h}^T|^2 D_2[m_{\nu_{v_h}}, m_{u_i}, m_W, m_W]. \quad (5.2)$$

Our parameter set leads that the contribution $\Delta C_{9,\ell}^{W/H^\pm} = -\Delta C_{10,\ell}^{W/H^\pm}$ in Eq. (5.2) is at negative 10^{-2} scale for both $\mu^+\mu^-$ and e^+e^- channels. This small LFU effect cannot be included in both C_V and C_U within Eq. (1.3) and is ignored for the approximation. Also we obtain $C_U^{\gamma(2)}$ around 0.01 and $C_V^{\chi^\pm(1)}$ around -0.01 in which the main contributions are from λ' diagrams. In summary, the LFU violating coefficient and the LFU coefficient can be represented by $C_V = C_V^{\chi^\pm(1)} + C_V^{\chi^\pm(2)}$ and $C_U = C_U^{\gamma(1)} + C_U^{\gamma(2)}$, respectively. We find that the factor $c_{mv}^{\mu L} = -g_2 V_{m1} \tilde{\mathcal{V}}_{v2}^T + V_{m2} Y_{2v}^T$ in Eq. (4.3) is also included in $C_V^{\chi^\pm(1)}$ and $C_V^{\chi^\pm(2)}$. Therefore, the large chiral mixing of sneutrinos will make some enhancements to both C_V and a_μ^{NP} simultaneously.

5.2 Explanations of $b \rightarrow s\ell^+\ell^-$ anomalies with $(g-2)_\mu$

In this part we will search for the common areas of these five variables, $m_{\tilde{L}_2}$, λ'_{223} , λ'_{233} , λ'_{323} and λ'_{333} , to explain $b \rightarrow s\ell^+\ell^-$ anomalies as well as $(g-2)_\mu$ deviations considering related constraints, in two fit scenarios mentioned in section 1. In scenario A, we fix $m_{\tilde{L}_3} = m_{\tilde{L}_2} - 50$ GeV which is benefit for satisfying the constraint of $B_s - \bar{B}_s$ mixing. In scenario B, we fix $m_{\tilde{L}_3} = m_{\tilde{L}_2}$. For the bounds of $m_{\tilde{L}_2}$ in LHC searches mentioned in section 4.7, we focus on $m_{\tilde{L}_2} \geq 370$ GeV which makes the mass of lightest charged slepton $m_{\tilde{l}_1}$ (sneutrino $m_{\tilde{\nu}_1}$) be above 318 (301) GeV in scenario A and $m_{\tilde{\nu}_1}$ be heavier than 100 GeV while $m_{\tilde{l}_1}$ be above 352 GeV in scenario B. In particular, we choose $k=3$ for a benchmark of the numerical calculation.

5.2.1 Explanations of $(g-2)_\mu$ anomalies

At first, we show the bound for $m_{\tilde{L}_2}$ with a_μ^{NP} in each scenario at figure 3, in which a_μ^{NP} can contribute to a_μ^{SM} increasing and accommodate the observed Δa_μ deviation from 4.2σ to 2σ level below. In scenario B, there are also allowed spaces at 1σ level. In scenario A, we obtain the allowed range $370 \leq m_{\tilde{L}_2} \leq 470$ GeV at 2σ level, and in scenario B there is a larger range of $370 \leq m_{\tilde{L}_2} \leq 820$ GeV at 2σ level as well as a range of $420 \leq m_{\tilde{L}_2} \leq 610$ GeV at 1σ level. Besides, we have calculated that a_e^{NP} can reach negative $\mathcal{O}(10^{-14})$ only in the case of $m_{\tilde{e}_R} \sim 100$ GeV in our parameter spaces.

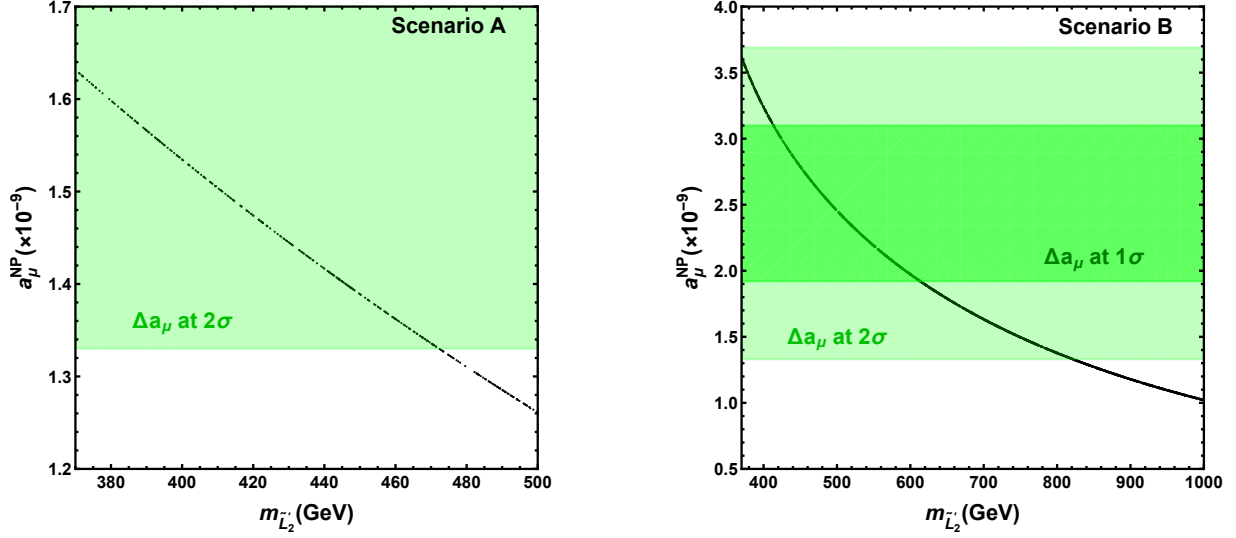


Figure 3: a_μ^{NP} varies with $m_{\tilde{L}_2'}$ in scenario A (left) and scenario B (right). The dark (light) green areas are $1(2)\sigma$ favored to explain the Δa_μ deviation.

5.2.2 Results in scenario A

Next we investigate $b \rightarrow s\ell^+\ell^-$ anomalies further with the parameter regions of $m_{\tilde{L}_2'}$ we have obtained above. In scenario A, C_U should be 0 as the definition. To make C_U cancel out, $\lambda_{323}^* \lambda'_{333}$ is figured out as the expression of $\lambda_{223}^* \lambda'_{233}$ and vice versa, and the constraints from $B_s - \bar{B}_s$ mixing and $B \rightarrow X_s \gamma$ will be mainly suppressed. Also the large m_{H^\pm} as 2 TeV and $m_{\tilde{u}_{Ri}}$ as 1.5 TeV avoid too strong bounds on the MSSM part of model from $B \rightarrow X_s \gamma$ decays. In figure 4, the common areas of $b \rightarrow s\ell^+\ell^-$ explanations under other bounds show a larger value and region of $\lambda_{223}^* \lambda'_{233}$ or $-\lambda_{323}^* \lambda'_{333}$ for a heavier $m_{\tilde{L}_2'}$. The values of $\lambda_{323}^* \lambda'_{333}$ always have the negative sign compared with the positive $\lambda_{223}^* \lambda'_{233}$, and their region sizes are nearly the same for the same value of $m_{\tilde{L}_2'}$. The results in scenario A show that $b \rightarrow s\ell^+\ell^-$ anomalies in both 1σ and 2σ fits can be explained.

Combined with considering the Δa_μ deviation, we find the final common region to explain the $b \rightarrow s\ell^+\ell^-$ and a_μ anomalies simultaneously at 2σ level which are shown by the points on the left of Δa_μ bound line in figure 4(b). The result provides the $m_{\tilde{L}_2'}$ range as $370 \text{ GeV} \leq m_{\tilde{L}_2'} \leq 470 \text{ GeV}$ and edge values of λ' combinations are collected in table 3.

5.2.3 Results in scenario B

In scenario B, the common scopes are shown at figure 5 and figure 6. Similar to scenario A, the values of allowed $\lambda_{323}^* \lambda'_{333}$ are always negative compared with the positive $\lambda_{223}^* \lambda'_{233}$ and the

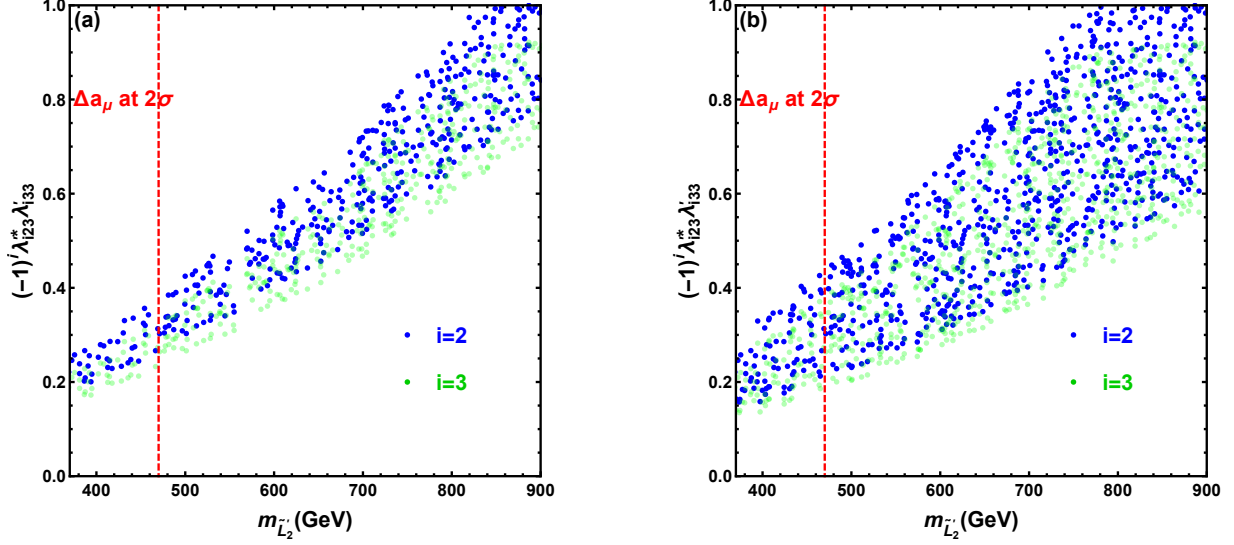


Figure 4: The common scopes of constraints with the fit level of rare B -meson decays as 1σ (left) and 2σ (right) in scenario A. The blue (green) points show $\lambda_{223}^* \lambda'_{233}$ ($-\lambda_{323}^* \lambda'_{333}$) varies with $m_{\tilde{L}'_2}$ and then $\lambda_{323}^* \lambda'_{333}$ ($\lambda_{223}^* \lambda'_{233}$) is derived. It should be paid attention to that among $\lambda_{223}^* \lambda'_{233}$ and $\lambda_{323}^* \lambda'_{333}$ there is only one independent variable in this scenario so the blue and green points are relevant. The area on the left of the red dashed line is allowed to be accordant with a_μ data at 2σ .

$m_{\tilde{L}'_2}$ [GeV]	$\lambda_{223}^* \lambda'_{233}$	$\lambda_{323}^* \lambda'_{333}$
370	[0.14, 0.30]	[-0.26, -0.12]
420	[0.17, 0.37]	[-0.32, -0.15]
470	[0.20, 0.44]	[-0.38, -0.18]

Table 3: The edge values of $\lambda_{223}^* \lambda'_{233}$ and $\lambda_{323}^* \lambda'_{333}$ related to different $m_{\tilde{L}'_2}$ for the simultaneous explanation of $b \rightarrow s \ell^+ \ell^-$ and a_μ anomalies at 2σ level in scenario A.

region sizes of their common scopes become larger as $m_{\tilde{L}'_2}$ varying heavier. As shown in figure 5, there exist areas to explain $b \rightarrow s \ell^+ \ell^-$ anomalies at 1σ level for rare B -meson decay fits, and the $B_s - \bar{B}_s$ mixing constrains mostly. While $B \rightarrow X_s \gamma$ decays provide no extra bounds when $m_{\tilde{L}'_2} \gtrsim 430$ GeV and even reaches TeV. When $m_{\tilde{L}'_2}$ blow around 430 GeV, 1σ explanations will not be viable, and $B \rightarrow X_s \gamma$ decays provide extra bounds versus $B_s - \bar{B}_s$ mixing. In figure 6(a), we compare the common region sizes for the different fixed $m_{\tilde{L}'_2}$ with each other and find that the deviation between the allowed region sizes of $\lambda_{223}^* \lambda'_{233}$ and $-\lambda_{323}^* \lambda'_{333}$ is small, up to around 0.1 scale. Thus we further fix them equalling to each other and show $\lambda_{223}^* \lambda'_{233}$ varying with increasing $m_{\tilde{L}'_2}$ only in figure 6(b) and find that, the 1σ favored fit requires $m_{\tilde{L}'_2} \gtrsim 550$ GeV and the region of 2σ fit has a broader size. When $m_{\tilde{L}'_2}$ below 550 GeV, there also exist common regions of 1σ fit while in these regions, $\lambda_{223}^* \lambda'_{233} + \lambda_{323}^* \lambda'_{333} \neq 0$.

Combined with a_μ data, the final common region of $400 \text{ GeV} \leq m_{\tilde{L}'_2} \leq 820 \text{ GeV}$ is required to explain the $b \rightarrow s\ell^+\ell^-$ and a_μ anomalies simultaneously at 2σ level and edge values of λ' combinations are collected in table 4.

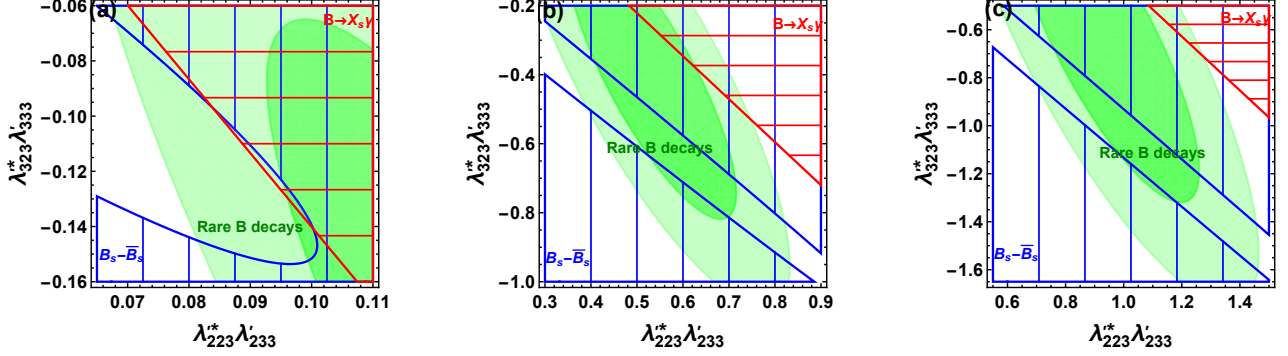


Figure 5: The regions of constraints in scenario B without a_μ data. The green regions are $1(2)\sigma$ favored ones with dark (light) opacity to satisfy the rare B -meson decay fits. At 2σ level, the hatched blue areas are excluded by $B_s - \bar{B}_s$ mixing and the hatched red areas are excluded by $B \rightarrow X_s \gamma$ decays. Besides, $m_{\tilde{L}'_3} = m_{\tilde{L}'_2}$ are fixed as 430 (left), 750 (middle) and 1000 GeV (right).

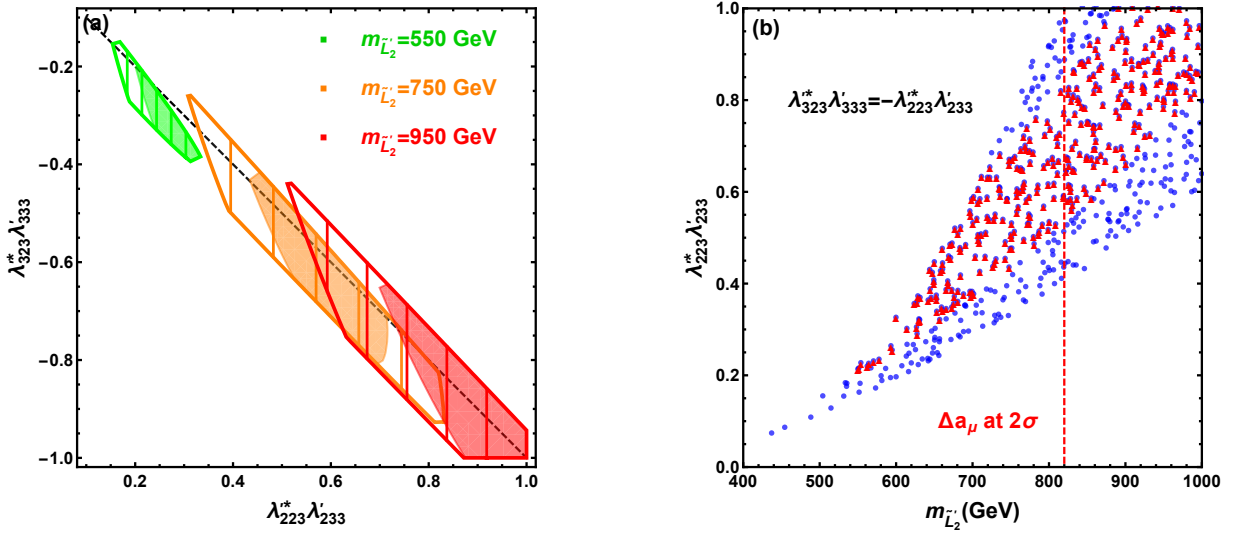


Figure 6: The common scopes of constraints in scenario B. Figure 6(a) shows the common scopes constrained by the rare B -meson decay fits at 1σ level denoted by painted areas and 2σ level denoted by hatched areas, combined with other process constraints at 2σ level for $m_{\tilde{L}'_3} = m_{\tilde{L}'_2} = 550$ (green), 750 (orange) and 950 GeV (red). Figure 6(b) shows the regions which satisfy the rare B -meson decay fits with being $1(2)\sigma$ favored under the assumption $\lambda_{323}^* \lambda_{333}' = -\lambda_{223}^* \lambda_{233}'$, denoted by red (blue) points, with other process constraints being considered. The area on the left of the red dashed line is allowed to be accordant with a_μ data at 2σ .

5.3 Predictions of $t \rightarrow cg$ decay

As the numerical discussions above, we have the final parameter spaces of $m_{\tilde{L}'_2}$ as well as the coupling combinations $\lambda_{223}^* \lambda'_{233}$ and $\lambda_{323}^* \lambda'_{333}$ to explain related LFU violating anomalies. While these variables also provide NP effects on the top decays $t \rightarrow cV(h)$.

We have checked that our final parameter spaces can satisfy the most recent upper limits on the branching ratios of $t \rightarrow cV(h)$ decays at LHC easily. The NP contributions to the branching ratios of $t \rightarrow cV(h)$ depend on the term $\tilde{\lambda}_{i2k}^* \tilde{\lambda}'_{i3k} f_{\tilde{L}_i}$ where $f_{\tilde{L}_i}$ stands for the loop integral including LH charged sleptons. And this term can be given by $\tilde{\lambda}_{i2k}^* \tilde{\lambda}'_{i3k} f_{\tilde{L}_i} \approx (\lambda_{i2k}^* \lambda'_{i3k} + |\lambda'_{i2k}|^2 K_{cb} + |\lambda'_{i3k}|^2 K_{cb}) f_{\tilde{L}_i}$. Because of cancelling out in $\lambda_{i2k}^* \lambda'_{i3k} f_{\tilde{L}_i}$, the hierarchical structure between λ'_{a2k} and λ'_{a3k} ($a = 2, 3$) is considered to make prominent contributions and we set the large λ'_{a3k} here. We keep restricting k as 3 and set $\lambda'_{233} = \lambda'_{333} = 2$ or 3.

In the following we show that the prediction values of $\mathcal{B}(t \rightarrow cg)_{\text{NP}}$ from the parameter spaces to explain $b \rightarrow s\ell^+\ell^-$ and a_μ anomalies can reach the sensitivity at the FCC-hh in figure 7. One can see that in scenario A, when $370 \text{ GeV} \leq m_{\tilde{L}'_2} \leq 440 \text{ GeV}$ and $\lambda'_{a33} = 3$, the prediction $\mathcal{B}(t \rightarrow cg)_{\text{NP}}$ is higher than the prospect upper limit 9.87×10^{-8} , at 100 TeV FCC-hh for the integrated luminosity of $\mathcal{L} = 10 \text{ ab}^{-1}$ of data through the triple-top signal [223], and the prediction in scenario B for the same λ'_{a33} can also reach this upper limit. When λ'_{a33} is set to be 2, the branching ratio is much lower and can not even reach the sensitivity at FCC-hh for the estimated $\mathcal{L} = 39 \text{ ab}^{-1}$ in both scenario A and B. We conclude that, at FCC-hh, this model signal on the $t \rightarrow cg$ transition has considerable possibilities to be found for sufficiently large λ'_{a33} , but the model can escape easily from the bound of this transition when the structure between λ'_{a23} and λ'_{a33} is not hierarchical enough.

$m_{\tilde{L}'_2} [\text{GeV}]$	$\lambda_{223}^* \lambda'_{233}$	$\lambda_{323}^* \lambda'_{333}$
420	[0.062, 0.086]	[-0.137, -0.063]
650	[0.22, 0.62]	[-0.70, -0.17]
820	[0.35, 1.00]	[-1.10, -0.30]

Table 4: The same as table 3 except for scenario B.

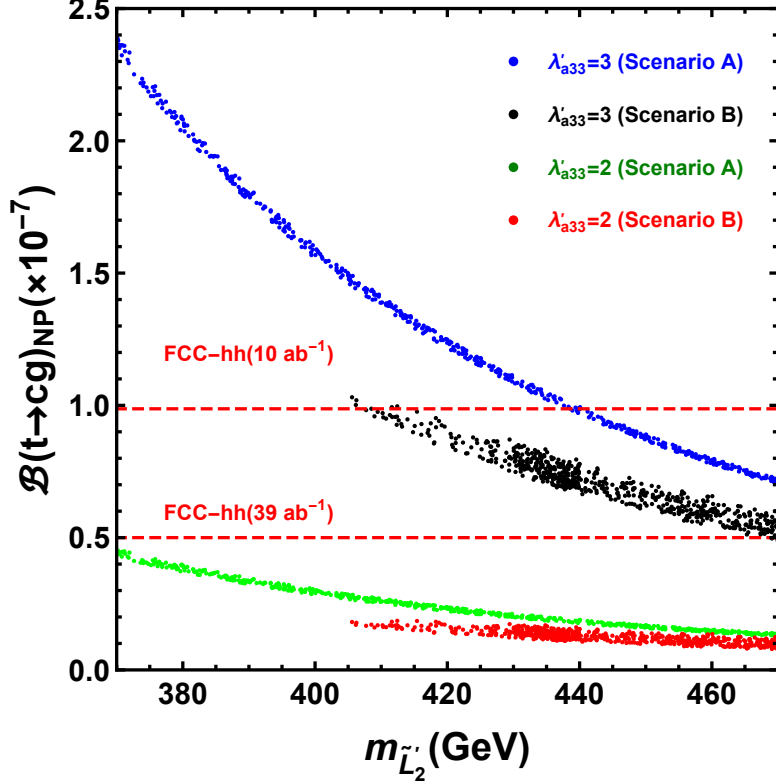


Figure 7: The predictions of $\mathcal{B}(t \rightarrow cg)_{\text{NP}}$ compared with the prospect upper limit at 100 TeV FCC-hh.

6 Conclusions

Recent measurements on the transition $b \rightarrow s\ell^+\ell^-$ reveal the deviations from SM predictions. The most motivative $R_K^{(*)}$ anomaly and anomalies from other observables like P'_5 , called $b \rightarrow s\ell^+\ell^-$ anomalies collectively, suggest the NP of LFU violation may exist. Besides, this NP may also affect the enduring muon anomalous magnetic moment, $(g-2)_\mu$ problem.

In this work, we have studied the chiral mixing effects of sneutrinos in the R -parity violating MSSM with inverse seesaw mechanisms to explore the explanation of $b \rightarrow s\ell^+\ell^-$ anomalies with $(g-2)_\mu$ problem simultaneously. Here all the one-loop contributions to $b \rightarrow s\ell^+\ell^-$ processes are scrutinized under the assumption of a single value k . Among them, the contributions of chiral mixing between LH and singlet (s)neutrinos within superpotential term $\lambda'_{ijk}\hat{L}_i\hat{Q}_j\hat{D}_k$ are given for the first time to our knowledge. To explain $b \rightarrow s\ell^+\ell^-$ anomalies in this model, two kinds of model-independent global fits are adopted. One is the single-parameter scenario of $C_{9,\mu}^{\text{NP}} = -C_{10,\mu}^{\text{NP}}$ and the other scenario is the double-parameter one that $(\pm)C_V$ contributes to the $C_{9(10),\mu}^{\text{NP}}$ part in $\mu^+\mu^-$ channel and C_U contributes to C_9^{NP} part in both $\mu^+\mu^-$ and e^+e^- channels. Then in the numerical analyses, we find that $b \rightarrow s\ell^+\ell^-$ and $(g-2)_\mu$ anomalies can

be explained simultaneously in both scenario A and B. The main constraints among related processes are from $B_s - \bar{B}_s$ mixing covering $B \rightarrow X_s \gamma$ decay mostly but the other tree-level and one-loop processes provide no effective bounds. At last we make a prospect that NP contributions to $t \rightarrow c g$ process can reach the sensitivity at FCC-hh in parts of the parameter spaces of this model.

Acknowledgements

We thank Yi-Lei Tang and Chengfeng Cai for valuable discussions. This work is supported in part by the National Natural Science Foundation of China under Grant No. 11875327, the Fundamental Research Funds for the Central Universities, and the Sun Yat-Sen University Science Foundation.

A One-loop box contributions in RPV-MSSMIS

In this appendix, we list the whole Wilson coefficients from the one-loop box diagrams of $b \rightarrow s \ell^+ \ell^-$ in RPV-MSSMIS without the extra assumption of a single value k .

The LH-quark-current contributions of chargino box diagrams to $b \rightarrow s \ell^+ \ell^-$ process are given by

$$\begin{aligned}
C_{9,\ell}^{\chi^\pm} = -C_{10,\ell}^{\chi^\pm} = & -\frac{\sqrt{2}\pi^2 i}{2G_F \eta_t e^2} \left(g_2^2 K_{i3} K_{i2}^* V_{m1}^* V_{n1} (g_2 V_{m1} \tilde{\mathcal{V}}_{v\ell}^{\mathcal{I}} - V_{m2} Y_{\ell v}^{\mathcal{I}}) \right. \\
& (g_2 V_{n1}^* \tilde{\mathcal{V}}_{v\ell}^{\mathcal{I}} - V_{n2}^* Y_{\ell v}^{\mathcal{I}}) D_2[m_{\tilde{\nu}_v^{\mathcal{I}}}, m_{\chi_m^\pm}, m_{\chi_n^\pm}, m_{\tilde{u}_{Li}}] \\
& + y_{u_i}^2 K_{i3} K_{i2}^* V_{m2}^* V_{n2} (g_2 V_{m1} \tilde{\mathcal{V}}_{v\ell}^{\mathcal{I}} - V_{m2} Y_{\ell v}^{\mathcal{I}}) \\
& (g_2 V_{n1}^* \tilde{\mathcal{V}}_{v\ell}^{\mathcal{I}} - V_{n2}^* Y_{\ell v}^{\mathcal{I}}) D_2[m_{\tilde{\nu}_v^{\mathcal{I}}}, m_{\chi_m^\pm}, m_{\chi_n^\pm}, m_{\tilde{u}_{Ri}}] \\
& - \lambda_{v3k}^{\mathcal{I}} \lambda_{v'2k}^{\mathcal{I}*} (g_2 V_{m1}^* \tilde{\mathcal{V}}_{v\ell}^{\mathcal{I}} - V_{m2}^* Y_{\ell v}^{\mathcal{I}}) (g_2 V_{m1} \tilde{\mathcal{V}}_{v'\ell}^{\mathcal{I}} - V_{m2} Y_{\ell v'}^{\mathcal{I}}) D_2[m_{\tilde{\nu}_v^{\mathcal{I}}}, m_{\tilde{\nu}_{v'}^{\mathcal{I}}}, m_{\chi_m^\pm}, m_{d_k}] \\
& - \tilde{\lambda}'_{\ell ik} \tilde{\lambda}'_{\ell jk}^* g_2^2 K_{i3} K_{j2}^* |V_{m1}|^2 D_2[m_{\tilde{u}_{Li}}, m_{\tilde{u}_{Lj}}, m_{\chi_m^\pm}, m_{d_k}] \\
& + \tilde{\lambda}'_{\ell ik} \lambda_{v2k}^{\mathcal{I}*} (g_2 K_{i3} V_{m1}^*) (g_2 V_{m1} \tilde{\mathcal{V}}_{v\ell}^{\mathcal{I}} - V_{m2} Y_{\ell v}^{\mathcal{I}}) D_2[m_{\tilde{\nu}_v^{\mathcal{I}}}, m_{\tilde{u}_{Li}}, m_{\chi_m^\pm}, m_{d_k}] \\
& \left. + \tilde{\lambda}'_{\ell ik}^* \lambda_{v3k}^{\mathcal{I}} (g_2 K_{i2}^* V_{m1}) (g_2 V_{m1}^* \tilde{\mathcal{V}}_{v\ell}^{\mathcal{I}} - V_{m2}^* Y_{\ell v}^{\mathcal{I}}) D_2[m_{\tilde{\nu}_v^{\mathcal{I}}}, m_{\tilde{u}_{Li}}, m_{\chi_m^\pm}, m_{d_k}] \right), \quad (\text{A.1})
\end{aligned}$$

where the Yukawa couplings $y_{u_i} = \sqrt{2}m_{u_i}/v_u$ and $Y_{\ell v}^{\mathcal{I}} = (Y_\nu)_{j\ell} \tilde{\mathcal{V}}_{v(j+3)}^{\mathcal{I}*}$. While the corresponding

RH-quark-current contributions are

$$C'_{9,\ell}{}^{\chi^\pm} = -C'_{10,\ell}{}^{\chi^\pm} = -\frac{\sqrt{2}\pi^2 i}{2G_F\eta_t e^2} \lambda_{vi2}^{\mathcal{I}} \lambda_{v'i3}^{\mathcal{I}*} (g_2 V_{m1}^* \tilde{\mathcal{V}}_{v\ell}^{\mathcal{I}} - V_{m2}^* Y_{\ell v}^{\mathcal{I}}) \\ (g_2 V_{m1} \tilde{\mathcal{V}}_{v'\ell}^{\mathcal{I}} - V_{m2} Y_{\ell v'}^{\mathcal{I}}) D_2[m_{\tilde{\nu}_v^{\mathcal{I}}}, m_{\tilde{\nu}_{v'}^{\mathcal{I}}}, m_{\chi_m^\pm}, m_{d_i}]. \quad (\text{A.2})$$

The contributions of W/H^\pm box diagrams to $b \rightarrow s\ell^+\ell^-$ process are given by

$$C_{9,\ell}^{W/H^\pm} = -C_{10,\ell}^{W/H^\pm} = -\frac{\sqrt{2}\pi^2 i}{2G_F\eta_t e^2} \left(y_{u_i}^2 K_{i3} K_{i2}^* Z_{H_{h2}}^2 Z_{H_{h'2}}^2 |Y_{\ell v}^{\mathcal{N}}|^2 D_2[m_{\nu_v}, m_{u_i}, m_{H_h}, m_{H_{h'}}] \right. \\ - 4g_2^2 m_{u_i} y_{u_i} m_{\nu_v} K_{i3} K_{i2}^* Z_{H_{h2}}^2 \text{Re}(\mathcal{V}_{v\ell} Y_{\ell v}^{\mathcal{N}*}) D_0[m_{\nu_v}, m_{u_i}, m_W, m_{H_h}] \\ + 5g_2^4 K_{i3} K_{i2}^* |\mathcal{V}_{v\ell}|^2 D_2[m_{\nu_v}, m_{u_i}, m_W, m_W] \\ + Z_{H_{h2}}^2 Y_{\ell v}^{\mathcal{N}*} Y_{\ell v'}^{\mathcal{N}} \lambda_{v'3k}^{\mathcal{N}} \lambda_{v'2k}^{\mathcal{N}*} D_2[m_{\nu_v}, m_{\nu_{v'}}, m_{H_h}, m_{\tilde{d}_{Rk}}] \\ - 2g_2^2 m_{\nu_v} m_{\nu_{v'}} \mathcal{V}_{v\ell}^* \mathcal{V}_{v'\ell} \lambda_{v'3k}^{\mathcal{N}} \lambda_{v'2k}^{\mathcal{N}*} D_0[m_{\nu_v}, m_{\nu_{v'}}, m_W, m_{\tilde{d}_{Rk}}] \\ + 2m_{\nu_v} m_{\nu_{v'}} Z_{H_{h2}}^2 Y_{\ell v}^{\mathcal{N}} Y_{\ell v'}^{\mathcal{N}*} \lambda_{v'3k}^{\mathcal{N}} \lambda_{v'2k}^{\mathcal{N}*} D_0[m_{\nu_v}, m_{\nu_{v'}}, m_{H_h}, m_{\tilde{d}_{Rk}}] \\ + 2m_{u_i} m_{u_j} y_{u_i} y_{u_j} K_{i3} K_{j2}^* Z_{H_{h2}}^2 \tilde{\lambda}'_{\ell ik} \tilde{\lambda}'_{\ell jk}^* D_0[m_{u_i}, m_{u_j}, m_{H_h}, m_{\tilde{d}_{Rk}}] \\ - g_2^2 \mathcal{V}_{v\ell} \mathcal{V}_{v'\ell}^* \lambda_{v'3k}^{\mathcal{N}} \lambda_{v'2k}^{\mathcal{N}*} D_2[m_{\nu_v}, m_{\nu_{v'}}, m_W, m_{\tilde{d}_{Rk}}] \\ - g_2^2 K_{i3} K_{j2}^* \tilde{\lambda}'_{\ell ik} \tilde{\lambda}'_{\ell jk}^* D_2[m_{u_i}, m_{u_j}, m_W, m_{\tilde{d}_{Rk}}] \\ - 2m_{u_i} y_{u_i} m_{\nu_v} K_{i3} Z_{H_{h2}}^2 Y_{\ell v}^{\mathcal{N}*} \tilde{\lambda}'_{\ell ik} \lambda_{v'2k}^{\mathcal{N}*} D_0[m_{u_i}, m_{\nu_v}, m_{H_h}, m_{\tilde{d}_{Rk}}] \\ - 2m_{u_i} y_{u_i} m_{\nu_v} K_{i2}^* Z_{H_{h2}}^2 Y_{\ell v}^{\mathcal{N}} \tilde{\lambda}'_{\ell ik} \lambda_{v'3k}^{\mathcal{N}} D_0[m_{u_i}, m_{\nu_v}, m_{H_h}, m_{\tilde{d}_{Rk}}] \\ + g_2^2 K_{i2}^* \mathcal{V}_{v\ell} \tilde{\lambda}'_{\ell ik}^* \lambda_{v'3k}^{\mathcal{N}} D_2[m_{u_i}, m_{\nu_v}, m_W, m_{\tilde{d}_{Rk}}] \\ + g_2^2 K_{i3} \mathcal{V}_{v\ell}^* \tilde{\lambda}'_{\ell ik} \lambda_{v'2k}^{\mathcal{N}*} D_2[m_{u_i}, m_{\nu_v}, m_W, m_{\tilde{d}_{Rk}}] \Big), \quad (\text{A.3})$$

$$C'_{9,\ell}{}^{W/H^\pm} = -C'_{10,\ell}{}^{W/H^\pm} = -\frac{\sqrt{2}\pi^2 i}{2G_F\eta_t e^2} \left(-2Z_{H_{h2}}^2 Y_{\ell v}^{\mathcal{N}*} Y_{\ell v'}^{\mathcal{N}} \lambda_{v'i2}^{\mathcal{N}} \lambda_{vi3}^{\mathcal{N}*} m_{\nu_v} m_{\nu_{v'}} D_0[m_{\nu_v}, m_{\nu_{v'}}, m_{H_h}, m_{\tilde{d}_{Li}}] \right. \\ - Z_{H_{h2}}^2 Y_{\ell v}^{\mathcal{N}} Y_{\ell v'}^{\mathcal{N}*} \lambda_{v'i2}^{\mathcal{N}} \lambda_{vi3}^{\mathcal{N}*} D_2[m_{\nu_v}, m_{\nu_{v'}}, m_{H_h}, m_{\tilde{d}_{Li}}] \\ + g_2^2 \mathcal{V}_{v\ell} \mathcal{V}_{v'\ell}^* \lambda_{v'i2}^{\mathcal{N}} \lambda_{vi3}^{\mathcal{N}*} D_2[m_{\nu_v}, m_{\nu_{v'}}, m_W, m_{\tilde{d}_{Li}}] \\ + 2g_2^2 \mathcal{V}_{v\ell} \mathcal{V}_{v'\ell}^* \lambda_{v'i2}^{\mathcal{N}} \lambda_{vi3}^{\mathcal{N}*} m_{\nu_v} m_{\nu_{v'}} D_0[m_{\nu_v}, m_{\nu_{v'}}, m_W, m_{\tilde{d}_{Li}}] \Big), \quad (\text{A.4})$$

where the mixing matrix elements $Z_{H_{12}} = -\sin\beta$, $Z_{H_{22}} = -\cos\beta$ with Goldstone mass $m_{H_1} = m_W$ and charged Higgs mass $m_{H_2} = m_{H^\pm}$ and $Y_{\ell v}^{\mathcal{N}} = (Y_\nu)_{j\ell} \mathcal{V}_{v(j+3)}^*$.

The contributions of $4\lambda'$ box diagrams to $b \rightarrow s\ell^+\ell^-$ process are given by

$$C'_{9,\ell}{}^{4\lambda'} = -C'_{10,\ell}{}^{4\lambda'} = -\frac{\sqrt{2}\pi^2 i}{2G_F\eta_t e^2} \left(\tilde{\lambda}'_{\ell ik} \tilde{\lambda}'_{\ell ik'}{}^* \lambda'_{v3k'}{}^{\mathcal{N}} \lambda'_{v2k}{}^{\mathcal{N}*} D_2[m_{\nu_v}, m_{u_i}, m_{\tilde{d}_{Rk}}, m_{\tilde{d}_{Rk'}}] \right. \\ \left. + \tilde{\lambda}'_{\ell ik} \tilde{\lambda}'_{\ell ik'}{}^* \lambda'_{v3k}{}^{\mathcal{I}} \lambda'_{v2k'}{}^{\mathcal{I}*} D_2[m_{\tilde{\nu}_v^{\mathcal{I}}}, m_{\tilde{u}_{Li}}, m_{d_k}, m_{d_{k'}}] \right), \quad (\text{A.5})$$

$$C'_{9,\ell}{}^{4\lambda'} = -C'_{10,\ell}{}^{4\lambda'} = -\frac{\sqrt{2}\pi^2 i}{2G_F\eta_t e^2} \left(\tilde{\lambda}'_{\ell ij} \tilde{\lambda}'_{\ell ij'}{}^* \lambda'_{vj2}{}^{\mathcal{N}} \lambda'_{vj'3}{}^{\mathcal{N}*} D_2[m_{\nu_v}, m_{u_i}, m_{\tilde{d}_{Lj}}, m_{\tilde{d}_{Lj'}}] \right. \\ \left. - \tilde{\lambda}'_{\ell j'k} \tilde{\lambda}'_{\ell jk}{}^* \tilde{\lambda}'_{ij2} \tilde{\lambda}'_{ij'3}{}^* (D_2[m_{l_i}, m_{\tilde{u}_{Lj}}, m_{\tilde{u}_{Lj'}}, m_{d_k}] + D_2[m_{\tilde{l}_{Li}}, m_{u_j}, m_{u_{j'}}, m_{\tilde{d}_{Rk}}]) \right). \quad (\text{A.6})$$

The contributions of neutralino box diagrams only contain RH-quark-current parts, which are given by

$$C'_{9,\ell}{}^{\chi^0} = -C'_{10,\ell}{}^{\chi^0} = -\frac{\sqrt{2}\pi^2 i}{2G_F\eta_t e^2} \left(\frac{1}{2} (g_1 N_{n1} + g_2 N_{n2})^2 \tilde{\lambda}'_{\ell i2} \tilde{\lambda}'_{\ell i3}{}^* D_2[m_{\tilde{l}_{L\ell}}, m_{\tilde{l}_{L\ell}}, m_{u_i}, m_{\chi_n^0}] \right. \\ \left. + \frac{2}{9} g_1^2 |N_{n1}|^2 \tilde{\lambda}'_{\ell i2} \tilde{\lambda}'_{\ell i3}{}^* D_2[m_{u_i}, m_{\chi_n^0}, m_{\tilde{s}_R}, m_{\tilde{b}_R}] \right. \\ \left. - \frac{1}{3} N_{n1} g_1 (g_1 N_{n1} + g_2 N_{n2}) \tilde{\lambda}'_{\ell i2} \tilde{\lambda}'_{\ell i3}{}^* (D_2[m_{\tilde{l}_{L\ell}}, m_{u_i}, m_{\chi_n^0}, m_{\tilde{s}_R}] + D_2[m_{\tilde{l}_{L\ell}}, m_{u_i}, m_{\chi_n^0}, m_{\tilde{b}_R}]) \right). \quad (\text{A.7})$$

References

- [1] **LHCb** Collaboration, R. Aaij et al., *Test of lepton universality in beauty-quark decays*, [arXiv:2103.11769](#).
- [2] **LHCb** Collaboration, R. Aaij et al., *Search for lepton-universality violation in $B^+ \rightarrow K^+ \ell^+ \ell^-$ decays*, *Phys. Rev. Lett.* **122** (2019), no. 19 191801, [[arXiv:1903.09252](#)].
- [3] **LHCb** Collaboration, R. Aaij et al., *Test of lepton universality with $B^0 \rightarrow K^{*0} \ell^+ \ell^-$ decays*, *JHEP* **08** (2017) 055, [[arXiv:1705.05802](#)].
- [4] **BELLE** Collaboration, S. Choudhury et al., *Test of lepton flavor universality and search for lepton flavor violation in $B \rightarrow K \ell \ell$ decays*, *JHEP* **03** (2021) 105, [[arXiv:1908.01848](#)].
- [5] **Belle** Collaboration, A. Abdesselam et al., *Test of Lepton-Flavor Universality in $B \rightarrow K^* \ell^+ \ell^-$ Decays at Belle*, *Phys. Rev. Lett.* **126** (2021), no. 16 161801, [[arXiv:1904.02440](#)].

- [6] **LHCb** Collaboration, R. Aaij et al., *Measurement of CP-Averaged Observables in the $B^0 \rightarrow K^{*0}\mu^+\mu^-$ Decay*, *Phys. Rev. Lett.* **125** (2020), no. 1 011802, [arXiv:2003.04831].
- [7] **LHCb** Collaboration, R. Aaij et al., *Angular analysis of the $B^0 \rightarrow K^{*0}\mu^+\mu^-$ decay using 3 fb^{-1} of integrated luminosity*, *JHEP* **02** (2016) 104, [arXiv:1512.04442].
- [8] **LHCb** Collaboration, R. Aaij et al., *Measurement of Form-Factor-Independent Observables in the Decay $B^0 \rightarrow K^{*0}\mu^+\mu^-$* , *Phys. Rev. Lett.* **111** (2013) 191801, [arXiv:1308.1707].
- [9] **CMS** Collaboration, V. Khachatryan et al., *Angular analysis of the decay $B^0 \rightarrow K^{*0}\mu^+\mu^-$ from pp collisions at $\sqrt{s} = 8\text{ TeV}$* , *Phys. Lett.* **B753** (2016) 424–448, [arXiv:1507.08126].
- [10] **ATLAS** Collaboration, M. Aaboud et al., *Angular analysis of $B_d^0 \rightarrow K^{*}\mu^+\mu^-$ decays in pp collisions at $\sqrt{s} = 8\text{ TeV}$ with the ATLAS detector*, *JHEP* **10** (2018) 047, [arXiv:1805.04000].
- [11] **Belle** Collaboration, S. Wehle et al., *Lepton-Flavor-Dependent Angular Analysis of $B \rightarrow K^{*}\ell^+\ell^-$* , *Phys. Rev. Lett.* **118** (2017), no. 11 111801, [arXiv:1612.05014].
- [12] **Belle** Collaboration, A. Abdesselam et al., *Angular analysis of $B^0 \rightarrow K^{*}(892)^0\ell^+\ell^-$* , in *Proceedings, LHCSki 2016 - A First Discussion of 13 TeV Results: Obergurgl, Austria, April 10-15, 2016*, 2016. arXiv:1604.04042.
- [13] J. Aebischer, W. Altmannshofer, D. Guadagnoli, M. Reboud, P. Stangl, and D. M. Straub, *B-decay discrepancies after Moriond 2019*, *Eur. Phys. J. C* **80** (2020), no. 3 252, [arXiv:1903.10434].
- [14] A. K. Alok, A. Dighe, S. Gangal, and D. Kumar, *Continuing search for new physics in $b \rightarrow s\mu\mu$ decays: two operators at a time*, *JHEP* **06** (2019) 089, [arXiv:1903.09617].
- [15] M. Algueró, B. Capdevila, A. Crivellin, S. Descotes-Genon, P. Masjuan, J. Matias, and J. Virto, *Emerging patterns of New Physics with and without Lepton Flavour Universal contributions*, *Eur. Phys. J.* **C79** (2019), no. 8 714, [arXiv:1903.09578].

- [16] M. Ciuchini, A. M. Coutinho, M. Fedele, E. Franco, A. Paul, L. Silvestrini, and M. Valli, *New Physics in $b \rightarrow s\ell^+\ell^-$ confronts new data on Lepton Universality*, *Eur. Phys. J. C* **79** (2019), no. 8 719, [[arXiv:1903.09632](#)].
- [17] A. Arbey, T. Hurth, F. Mahmoudi, D. M. Santos, and S. Neshatpour, *Update on the $b \rightarrow s$ anomalies*, *Phys. Rev. D* **100** (2019), no. 1 015045, [[arXiv:1904.08399](#)].
- [18] K. Kowalska, D. Kumar, and E. M. Sessolo, *Implications for new physics in $b \rightarrow s\mu\mu$ transitions after recent measurements by Belle and LHCb*, *Eur. Phys. J. C* **79** (2019), no. 10 840, [[arXiv:1903.10932](#)].
- [19] B. Capdevila, U. Laa, and G. Valencia, *Fitting in or odd one out? Pulls vs residual responses in $b \rightarrow s\ell^+\ell^-$* , [arXiv:1908.03338](#).
- [20] S. Bhattacharya, A. Biswas, S. Nandi, and S. K. Patra, *Exhaustive model selection in $b \rightarrow s\ell\ell$ decays: Pitting cross-validation against the Akaike information criterion*, *Phys. Rev. D* **101** (2020), no. 5 055025, [[arXiv:1908.04835](#)].
- [21] F. Munir Bhutta, Z.-R. Huang, C.-D. Lü, M. A. Paracha, and W. Wang, *New Physics in $b \rightarrow s\ell\ell$ anomalies and its implications for the complementary neutral current decays*, [arXiv:2009.03588](#).
- [22] A. Biswas, S. Nandi, S. K. Patra, and I. Ray, *New physics in $b \rightarrow s\ell\ell$ decays with complex Wilson coefficients*, *Nucl. Phys. B* **969** (2021) 115479, [[arXiv:2004.14687](#)].
- [23] J. Alda, J. Guasch, and S. Peñaranda, *Anomalies in B mesons decays: A phenomenological approach*, [arXiv:2012.14799](#).
- [24] A. Carvunis, F. Dettori, S. Gangal, D. Guadagnoli, and C. Normand, *On the effective lifetime of $B_s \rightarrow \mu\mu\gamma$* , [arXiv:2102.13390](#).
- [25] L.-S. Geng, B. Grinstein, S. Jäger, S.-Y. Li, J. Martin Camalich, and R.-X. Shi, *Implications of new evidence for lepton-universality violation in $b \rightarrow s\ell^+\ell^-$ decays*, *Phys. Rev. D* **104** (2021), no. 3 035029, [[arXiv:2103.12738](#)].
- [26] S.-Y. Li, R.-X. Shi, and L.-S. Geng, *Possible strategy of discriminating 1D new physics solutions in $b \rightarrow s\ell\ell$ decays after Moriond 2021*, [arXiv:2105.06768](#).

- [27] A. Angelescu, D. Bećirević, D. A. Faroughy, F. Jaffredo, and O. Sumensari, *Single leptoquark solutions to the B-physics anomalies*, *Phys. Rev. D* **104** (2021), no. 5 055017, [arXiv:2103.12504].
- [28] W. Altmannshofer and P. Stangl, *New Physics in Rare B Decays after Moriond 2021*, arXiv:2103.13370.
- [29] C. Cornella, D. A. Faroughy, J. Fuentes-Martin, G. Isidori, and M. Neubert, *Reading the footprints of the B-meson flavor anomalies*, *JHEP* **08** (2021) 050, [arXiv:2103.16558].
- [30] J. Kriewald, C. Hati, J. Orloff, and A. M. Teixeira, *Leptoquarks facing flavour tests and $b \rightarrow s\ell\ell$ after Moriond 2021*, in *55th Rencontres de Moriond on Electroweak Interactions and Unified Theories*, 3, 2021. arXiv:2104.00015.
- [31] G. Isidori, D. Lancierini, P. Owen, and N. Serra, *On the significance of new physics in $b \rightarrow s\ell^+\ell^-$ decays*, *Phys. Lett. B* **822** (2021) 136644, [arXiv:2104.05631].
- [32] M. Algueró, B. Capdevila, S. Descotes-Genon, J. Matias, and M. Novoa-Brunet, *$b \rightarrow s\ell\ell$ global fits after Moriond 2021 results*, in *55th Rencontres de Moriond on Electroweak Interactions and Unified Theories*, 4, 2021. arXiv:2104.08921.
- [33] T. Hurth, F. Mahmoudi, D. M. Santos, and S. Neshatpour, *More Indications for Lepton Nonuniversality in $b \rightarrow s\ell^+\ell^-$* , arXiv:2104.10058.
- [34] P. F. Perez, C. Murgui, and A. D. Plascencia, *Leptoquarks and matter unification: Flavor anomalies and the muon $g - 2$* , *Phys. Rev. D* **104** (2021), no. 3 035041, [arXiv:2104.11229].
- [35] J. Alda, J. Guasch, and S. Penaranda, *Anomalies in B mesons decays: Present status and future collider prospects*, in *International Workshop on Future Linear Colliders*, 5, 2021. arXiv:2105.05095.
- [36] R. Bause, H. Gisbert, M. Golz, and G. Hiller, *Interplay of dineutrino modes with semileptonic rare B-decays*, arXiv:2109.01675.
- [37] **LHCb** Collaboration, R. Aaij et al., *Angular Analysis of the $B^+ \rightarrow K^{*+}\mu^+\mu^-$ Decay*, *Phys. Rev. Lett.* **126** (2021), no. 16 161802, [arXiv:2012.13241].

- [38] **LHCb** Collaboration, R. Aaij et al., *Branching fraction measurements of the rare $B_s^0 \rightarrow \phi \mu^+ \mu^-$ and $B_s^0 \rightarrow f_2'(1525) \mu^+ \mu^-$ decays*, [arXiv:2105.14007](#).
- [39] **LHCb** Collaboration, R. Aaij et al., *Angular analysis and differential branching fraction of the decay $B_s^0 \rightarrow \phi \mu^+ \mu^-$* , *JHEP* **09** (2015) 179, [[arXiv:1506.08777](#)].
- [40] **CMS** Collaboration, A. M. Sirunyan et al., *Measurement of properties of $B_s^0 \rightarrow \mu^+ \mu^-$ decays and search for $B^0 \rightarrow \mu^+ \mu^-$ with the CMS experiment*, *JHEP* **04** (2020) 188, [[arXiv:1910.12127](#)].
- [41] **LHCb** Collaboration, R. Aaij et al., *Measurement of the $B_s^0 \rightarrow \mu^+ \mu^-$ decay properties and search for the $B^0 \rightarrow \mu^+ \mu^-$ and $B_s^0 \rightarrow \mu^+ \mu^- \gamma$ decays*, [arXiv:2108.09283](#).
- [42] **LHCb** Collaboration, R. Aaij et al., *Analysis of neutral B -meson decays into two muons*, [arXiv:2108.09284](#).
- [43] N. G. Deshpande and X.-G. He, *Consequences of R -parity violating interactions for anomalies in $\bar{B} \rightarrow D^{(*)} \tau \bar{\nu}$ and $b \rightarrow s \mu^+ \mu^-$* , *Eur. Phys. J.* **C77** (2017), no. 2 134, [[arXiv:1608.04817](#)].
- [44] D. Das, C. Hati, G. Kumar, and N. Mahajan, *Scrutinizing R -parity violating interactions in light of $R_{K^{(*)}}$ data*, *Phys. Rev.* **D96** (2017), no. 9 095033, [[arXiv:1705.09188](#)].
- [45] K. Earl and T. Grégoire, *Contributions to $b \rightarrow s \ell \ell$ Anomalies from R -Parity Violating Interactions*, *JHEP* **08** (2018) 201, [[arXiv:1806.01343](#)].
- [46] Q.-Y. Hu and L.-L. Huang, *Explaining $b \rightarrow s \ell^+ \ell^-$ data by sneutrinos in the R -parity violating MSSM*, *Phys. Rev. D* **101** (2020), no. 3 035030, [[arXiv:1912.03676](#)].
- [47] Q.-Y. Hu, Y.-D. Yang, and M.-D. Zheng, *Revisiting the B -physics anomalies in R -parity violating MSSM*, *Eur. Phys. J. C* **80** (2020), no. 5 365, [[arXiv:2002.09875](#)].
- [48] W. Altmannshofer, P. B. Dev, A. Soni, and Y. Sui, *Addressing $R_{D^{(*)}}$, $R_{K^{(*)}}$, muon $g - 2$ and ANITA anomalies in a minimal R -parity violating supersymmetric framework*, *Phys. Rev. D* **102** (2020), no. 1 015031, [[arXiv:2002.12910](#)].
- [49] P. Minkowski, *$\mu \rightarrow e \gamma$ at a Rate of One Out of 10^9 Muon Decays?*, *Phys. Lett. B* **67** (1977) 421–428.

- [50] O. Sawada and A. Sugamoto, eds., *Proceedings: Workshop on the Unified Theories and the Baryon Number in the Universe: Tsukuba, Japan, February 13-14, 1979*, (Tsukuba, Japan), Natl.Lab.High Energy Phys., 1979.
- [51] M. Gell-Mann, P. Ramond, and R. Slansky, *Complex Spinors and Unified Theories*, *Conf. Proc. C* **790927** (1979) 315–321, [[arXiv:1306.4669](#)].
- [52] R. N. Mohapatra and G. Senjanovic, *Neutrino Mass and Spontaneous Parity Nonconservation*, *Phys. Rev. Lett.* **44** (1980) 912.
- [53] J. Schechter and J. W. F. Valle, *Neutrino Masses in $SU(2) \times U(1)$ Theories*, *Phys. Rev. D* **22** (1980) 2227.
- [54] J. Schechter and J. W. F. Valle, *Neutrino Decay and Spontaneous Violation of Lepton Number*, *Phys. Rev. D* **25** (1982) 774.
- [55] G. Lazarides, Q. Shafi, and C. Wetterich, *Proton Lifetime and Fermion Masses in an $SO(10)$ Model*, *Nucl. Phys. B* **181** (1981) 287–300.
- [56] S. Khalil, *Explaining the R_K and R_{K^*} Anomalies With Right-handed Sneutrino*, *J. Phys. G* **45** (2018), no. 12 125004, [[arXiv:1706.07337](#)].
- [57] S.-P. Li, X.-Q. Li, Y.-D. Yang, and X. Zhang, *$R_{D^{(*)}}$, $R_{K^{(*)}}$ and neutrino mass in the 2HDM-III with right-handed neutrinos*, *JHEP* **09** (2018) 149, [[arXiv:1807.08530](#)].
- [58] L. Delle Rose, S. Khalil, S. J. D. King, and S. Moretti, *R_K and R_{K^*} in an Aligned 2HDM with Right-Handed Neutrinos*, *Phys. Rev. D* **101** (2020), no. 11 115009, [[arXiv:1903.11146](#)].
- [59] L. T. Hue, A. B. Arbuzov, N. T. K. Ngan, and H. N. Long, *Probing neutrino and Higgs sectors in $SU(2)_1 \times SU(2)_2 \times U(1)_Y$ model with lepton-flavor non-universality*, *Eur. Phys. J. C* **77** (2017), no. 5 346, [[arXiv:1611.06801](#)].
- [60] D. Bhatia, S. Chakraborty, and A. Dighe, *Neutrino mixing and R_K anomaly in $U(1)_X$ models: a bottom-up approach*, *JHEP* **03** (2017) 117, [[arXiv:1701.05825](#)].
- [61] P. Ko, T. Nomura, and H. Okada, *A flavor dependent gauge symmetry, Predictive radiative seesaw and $LHCb$ anomalies*, *Phys. Lett. B* **772** (2017) 547–552, [[arXiv:1701.05788](#)].

- [62] D. N. Dinh, L. Merlo, S. T. Petcov, and R. Vega-Álvarez, *Revisiting Minimal Lepton Flavour Violation in the Light of Leptonic CP Violation*, *JHEP* **07** (2017) 089, [[arXiv:1705.09284](#)].
- [63] C.-W. Chiang, X.-G. He, J. Tandean, and X.-B. Yuan, *$R_{K^{(*)}}$ and related $b \rightarrow s\ell\bar{\ell}$ anomalies in minimal flavor violation framework with Z' boson*, *Phys. Rev. D* **96** (2017), no. 11 115022, [[arXiv:1706.02696](#)].
- [64] S. Antusch, C. Hohl, S. F. King, and V. Susic, *Non-universal Z' from $SO(10)$ GUTs with vector-like family and the origin of neutrino masses*, *Nucl. Phys. B* **934** (2018) 578–605, [[arXiv:1712.05366](#)].
- [65] S. F. King, *$R_{K^{(*)}}$ and the origin of Yukawa couplings*, *JHEP* **09** (2018) 069, [[arXiv:1806.06780](#)].
- [66] J. Heeck and D. Teresi, *Pati-Salam explanations of the B-meson anomalies*, *JHEP* **12** (2018) 103, [[arXiv:1808.07492](#)].
- [67] D. Borah, L. Mukherjee, and S. Nandi, *Low scale $U(1)_X$ gauge symmetry as an origin of dark matter, neutrino mass and flavour anomalies*, *JHEP* **12** (2020) 052, [[arXiv:2007.13778](#)].
- [68] J.-Y. Cen, Y. Cheng, X.-G. He, and J. Sun, *Flavor Specific $U(1)_{B_q-L_\mu}$ Gauge Model for Muon $g-2$ and $b \rightarrow s\bar{\mu}\mu$ Anomalies*, [arXiv:2104.05006](#).
- [69] J. S. Alvarado, S. F. Mantilla, R. Martinez, and F. Ochoa, *A non-universal $U(1)_X$ extension to the Standard Model to study the B meson anomaly and muon $g-2$* , [arXiv:2105.04715](#).
- [70] B. Dutta, S. Ghosh, P. Huang, and J. Kumar, *Explaining $g_\mu - 2$ and $R_{K^{(*)}}$ using the light mediators of $U(1)_{T3R}$* , [arXiv:2105.07655](#).
- [71] A. Greljo, P. Stangl, and A. E. Thomsen, *A Model of Muon Anomalies*, *Phys. Lett. B* **820** (2021) 136554, [[arXiv:2103.13991](#)].
- [72] A. Greljo, Y. Soreq, P. Stangl, A. E. Thomsen, and J. Zupan, *Muonic Force Behind Flavor Anomalies*, [arXiv:2107.07518](#).

- [73] D. Bhatia, N. Desai, and A. Dighe, *Frugal $U(1)_X$ models with non-minimal flavor violation for $b \rightarrow s\ell\ell$ anomalies and neutrino mixing*, [arXiv:2109.07093](#).
- [74] I. Esteban, M. Gonzalez-Garcia, M. Maltoni, T. Schwetz, and A. Zhou, *The fate of hints: updated global analysis of three-flavor neutrino oscillations*, *JHEP* **09** (2020) 178, [[arXiv:2007.14792](#)].
- [75] R. N. Mohapatra, *Mechanism for Understanding Small Neutrino Mass in Superstring Theories*, *Phys. Rev. Lett.* **56** (1986) 561–563.
- [76] R. N. Mohapatra and J. W. F. Valle, *Neutrino Mass and Baryon Number Nonconservation in Superstring Models*, *Phys. Rev. D* **34** (1986) 1642.
- [77] N. Escudero, D. E. Lopez-Fogliani, C. Munoz, and R. Ruiz de Austri, *Analysis of the parameter space and spectrum of the $\mu\nu$ SSM*, *JHEP* **12** (2008) 099, [[arXiv:0810.1507](#)].
- [78] J. Fidalgo and C. Munoz, *The $\mu\nu$ SSM with an Extra $U(1)$* , *JHEP* **04** (2012) 090, [[arXiv:1111.2836](#)].
- [79] D. E. Lopez-Fogliani and C. Munoz, *On a reinterpretation of the Higgs field in supersymmetry and a proposal for new quarks*, *Phys. Lett. B* **771** (2017) 136–141, [[arXiv:1701.02652](#)].
- [80] **BaBar** Collaboration, J. P. Lees et al., *Evidence for an excess of $\bar{B} \rightarrow D^{(*)}\tau^-\bar{\nu}_\tau$ decays*, *Phys. Rev. Lett.* **109** (2012) 101802, [[arXiv:1205.5442](#)].
- [81] **BaBar** Collaboration, J. P. Lees et al., *Measurement of an Excess of $\bar{B} \rightarrow D^{(*)}\tau^-\bar{\nu}_\tau$ Decays and Implications for Charged Higgs Bosons*, *Phys. Rev.* **D88** (2013), no. 7 072012, [[arXiv:1303.0571](#)].
- [82] **Belle** Collaboration, M. Huschle et al., *Measurement of the branching ratio of $\bar{B} \rightarrow D^{(*)}\tau^-\bar{\nu}_\tau$ relative to $\bar{B} \rightarrow D^{(*)}\ell^-\bar{\nu}_\ell$ decays with hadronic tagging at Belle*, *Phys. Rev.* **D92** (2015), no. 7 072014, [[arXiv:1507.03233](#)].
- [83] **Belle** Collaboration, S. Hirose et al., *Measurement of the τ lepton polarization and $R(D^*)$ in the decay $\bar{B} \rightarrow D^*\tau^-\bar{\nu}_\tau$* , *Phys. Rev. Lett.* **118** (2017), no. 21 211801, [[arXiv:1612.00529](#)].

- [84] **Belle** Collaboration, S. Hirose et al., *Measurement of the τ lepton polarization and $R(D^*)$ in the decay $\bar{B} \rightarrow D^* \tau^- \bar{\nu}_\tau$ with one-prong hadronic τ decays at Belle*, *Phys. Rev. D* **97** (2018), no. 1 012004, [[arXiv:1709.00129](#)].
- [85] **Belle** Collaboration, G. Caria et al., *Measurement of $\mathcal{R}(D)$ and $\mathcal{R}(D^*)$ with a semileptonic tagging method*, *Phys. Rev. Lett.* **124** (2020), no. 16 161803, [[arXiv:1910.05864](#)].
- [86] **LHCb** Collaboration, R. Aaij et al., *Measurement of the ratio of branching fractions $\mathcal{B}(\bar{B}^0 \rightarrow D^{*+} \tau^- \bar{\nu}_\tau) / \mathcal{B}(\bar{B}^0 \rightarrow D^{*+} \mu^- \bar{\nu}_\mu)$* , *Phys. Rev. Lett.* **115** (2015), no. 11 111803, [[arXiv:1506.08614](#)]. [Erratum: *Phys. Rev. Lett.* 115, no. 15, 159901 (2015)].
- [87] **LHCb** Collaboration, R. Aaij et al., *Measurement of the ratio of the $B^0 \rightarrow D^{*-} \tau^+ \nu_\tau$ and $B^0 \rightarrow D^{*-} \mu^+ \nu_\mu$ branching fractions using three-prong τ -lepton decays*, *Phys. Rev. Lett.* **120** (2018), no. 17 171802, [[arXiv:1708.08856](#)].
- [88] **LHCb** Collaboration, R. Aaij et al., *Test of Lepton Flavor Universality by the measurement of the $B^0 \rightarrow D^{*-} \tau^+ \nu_\tau$ branching fraction using three-prong τ decays*, *Phys. Rev. D* **97** (2018), no. 7 072013, [[arXiv:1711.02505](#)].
- [89] **HFLAV** Collaboration, Y. S. Amhis et al., *Averages of b -hadron, c -hadron, and τ -lepton properties as of 2018*, *Eur. Phys. J. C* **81** (2021), no. 3 226, [[arXiv:1909.12524](#)].
- [90] D. Bigi and P. Gambino, *Revisiting $B \rightarrow D \ell \nu$* , *Phys. Rev. D* **94** (2016), no. 9 094008, [[arXiv:1606.08030](#)].
- [91] F. U. Bernlochner, Z. Ligeti, M. Papucci, and D. J. Robinson, *Combined analysis of semileptonic B decays to D and D^* : $R(D^{(*)})$, $|V_{cb}|$, and new physics*, *Phys. Rev. D* **95** (2017), no. 11 115008, [[arXiv:1703.05330](#)]. [erratum: *Phys. Rev. D* 97, no. 5, 059902 (2018)].
- [92] D. Bigi, P. Gambino, and S. Schacht, *$R(D^*)$, $|V_{cb}|$, and the Heavy Quark Symmetry relations between form factors*, *JHEP* **11** (2017) 061, [[arXiv:1707.09509](#)].
- [93] S. Jaiswal, S. Nandi, and S. K. Patra, *Extraction of $|V_{cb}|$ from $B \rightarrow D^{(*)} \ell \nu_\ell$ and the Standard Model predictions of $R(D^{(*)})$* , *JHEP* **12** (2017) 060, [[arXiv:1707.09977](#)].

- [94] P. Gambino, M. Jung, and S. Schacht, *The V_{cb} puzzle: An update*, *Phys. Lett. B* **795** (2019) 386–390, [[arXiv:1905.08209](#)].
- [95] M. Bordone, M. Jung, and D. van Dyk, *Theory determination of $\bar{B} \rightarrow D^{(*)} \ell^- \bar{\nu}$ form factors at $\mathcal{O}(1/m_c^2)$* , *Eur. Phys. J. C* **80** (2020), no. 2 74, [[arXiv:1908.09398](#)].
- [96] S. Jaiswal, S. Nandi, and S. K. Patra, *Updates on extraction of $|V_{cb}|$ and SM prediction of $R(D^*)$ in $B \rightarrow D^* \ell \nu_\ell$ decays*, *JHEP* **06** (2020) 165, [[arXiv:2002.05726](#)].
- [97] K. Cheung, Z.-R. Huang, H.-D. Li, C.-D. Lü, Y.-N. Mao, and R.-Y. Tang, *Revisit to the $b \rightarrow c \tau \nu$ transition: In and beyond the SM*, *Nucl. Phys. B* **965** (2021) 115354, [[arXiv:2002.07272](#)].
- [98] H.-M. Choi, *Self-consistent light-front quark model analysis of $B \rightarrow D \ell \nu_\ell$ transition form factors*, *Phys. Rev. D* **103** (2021), no. 7 073004, [[arXiv:2102.02015](#)].
- [99] S. Iguro and R. Watanabe, *Bayesian fit analysis to full distribution data of $\bar{B} \rightarrow D^{(*)} \ell \bar{\nu} : |V_{cb}|$ determination and new physics constraints*, *JHEP* **08** (2020), no. 08 006, [[arXiv:2004.10208](#)].
- [100] K. Hara, *$R(D)$ and $R(D^*)$ at Belle*, *PoS* **377** (2020) 041.
- [101] **Muon g-2** Collaboration, B. Abi et al., *Measurement of the Positive Muon Anomalous Magnetic Moment to 0.46 ppm*, *Phys. Rev. Lett.* **126** (4, 2021) 2021, [[arXiv:2104.03281](#)].
- [102] **Muon g-2** Collaboration, T. Albahri et al., *Measurement of the anomalous precession frequency of the muon in the Fermilab Muon g-2 experiment*, *Phys. Rev. D* **103** (2021) 072002, [[arXiv:2104.03247](#)].
- [103] **Muon g-2** Collaboration, T. Albahri et al., *Magnetic Field Measurement and Analysis for the Muon g-2 Experiment at Fermilab*, *Phys. Rev. A* **103** (2021) 042208, [[arXiv:2104.03201](#)].
- [104] T. Aoyama et al., *The anomalous magnetic moment of the muon in the Standard Model*, *Phys. Rept.* **887** (2020) 1–166, [[arXiv:2006.04822](#)].
- [105] S. Borsanyi et al., *Leading hadronic contribution to the muon magnetic moment from lattice QCD*, *Nature* **593** (2021), no. 7857 51–55, [[arXiv:2002.12347](#)].

- [106] G. Colangelo, M. Hoferichter, and P. Stoffer, *Two-pion contribution to hadronic vacuum polarization*, *JHEP* **02** (2019) 006, [[arXiv:1810.00007](#)].
- [107] M. Davier, A. Hoecker, B. Malaescu, and Z. Zhang, *A new evaluation of the hadronic vacuum polarisation contributions to the muon anomalous magnetic moment and to $\alpha(m_Z^2)$* , *Eur. Phys. J. C* **80** (2020), no. 3 241, [[arXiv:1908.00921](#)]. [Erratum: *Eur.Phys.J.C* 80, 410 (2020)].
- [108] A. Keshavarzi, D. Nomura, and T. Teubner, *$g - 2$ of charged leptons, $\alpha(M_Z^2)$, and the hyperfine splitting of muonium*, *Phys. Rev. D* **101** (2020), no. 1 014029, [[arXiv:1911.00367](#)].
- [109] M. Hoferichter, B.-L. Hoid, and B. Kubis, *Three-pion contribution to hadronic vacuum polarization*, *JHEP* **08** (2019) 137, [[arXiv:1907.01556](#)].
- [110] A. Crivellin, M. Hoferichter, C. A. Manzari, and M. Montull, *Hadronic Vacuum Polarization: $(g - 2)_\mu$ versus Global Electroweak Fits*, *Phys. Rev. Lett.* **125** (2020), no. 9 091801, [[arXiv:2003.04886](#)].
- [111] A. Keshavarzi, W. J. Marciano, M. Passera, and A. Sirlin, *Muon $g - 2$ and $\Delta\alpha$ connection*, *Phys. Rev. D* **102** (2020), no. 3 033002, [[arXiv:2006.12666](#)].
- [112] E. de Rafael, *Constraints between $\Delta\alpha_{\text{had}}(M_Z^2)$ and $(g_\mu - 2)_{\text{HVP}}$* , *Phys. Rev. D* **102** (2020), no. 5 056025, [[arXiv:2006.13880](#)].
- [113] B. Malaescu and M. Schott, *Impact of correlations between a_μ and α_{QED} on the EW fit*, *Eur. Phys. J. C* **81** (2021), no. 1 46, [[arXiv:2008.08107](#)].
- [114] **Muon g-2** Collaboration, G. W. Bennett et al., *Final Report of the Muon E821 Anomalous Magnetic Moment Measurement at BNL*, *Phys. Rev.* **D73** (2006) 072003, [[hep-ex/0602035](#)].
- [115] D. Hanneke, S. F. Hoogerheide, and G. Gabrielse, *Cavity Control of a Single-Electron Quantum Cyclotron: Measuring the Electron Magnetic Moment*, *Phys. Rev. A* **83** (2011) 052122, [[arXiv:1009.4831](#)].

- [116] T. Aoyama, T. Kinoshita, and M. Nio, *Revised and Improved Value of the QED Tenth-Order Electron Anomalous Magnetic Moment*, *Phys. Rev. D* **97** (2018), no. 3 036001, [[arXiv:1712.06060](#)].
- [117] R. H. Parker, C. Yu, W. Zhong, B. Estey, and H. Müller, *Measurement of the fine-structure constant as a test of the Standard Model*, *Science* **360** (2018) 191, [[arXiv:1812.04130](#)].
- [118] L. Morel, Z. Yao, P. Cladé, and S. Guellati-Khélifa, *Determination of the fine-structure constant with an accuracy of 81 parts per trillion*, *Nature* **588** (2020), no. 7836 61–65.
- [119] A. Gérardin, *The anomalous magnetic moment of the muon: status of Lattice QCD calculations*, *Eur. Phys. J. A* **57** (2021), no. 4 116, [[arXiv:2012.03931](#)].
- [120] J. Hisano and K. Tobe, *Neutrino masses, muon $g-2$, and lepton flavor violation in the supersymmetric seesaw model*, *Phys. Lett. B* **510** (2001) 197–204, [[hep-ph/0102315](#)].
- [121] J. E. Kim, B. Kyae, and H. M. Lee, *Effective supersymmetric theory and $(g-2)$ (muon with R -parity violation*, *Phys. Lett. B* **520** (2001) 298–306, [[hep-ph/0103054](#)].
- [122] S. P. Martin and J. D. Wells, *Muon Anomalous Magnetic Dipole Moment in Supersymmetric Theories*, *Phys. Rev. D* **64** (2001) 035003, [[hep-ph/0103067](#)].
- [123] D. Stockinger, *The Muon Magnetic Moment and Supersymmetry*, *J. Phys. G* **34** (2007) R45–R92, [[hep-ph/0609168](#)].
- [124] A. S. Belyaev, J. E. Camargo-Molina, S. F. King, D. J. Miller, A. P. Morais, and P. B. Schaefers, *A to Z of the Muon Anomalous Magnetic Moment in the MSSM with Pati-Salam at the GUT scale*, *JHEP* **06** (2016) 142, [[arXiv:1605.02072](#)].
- [125] M. Yamaguchi and W. Yin, *A novel approach to finely tuned supersymmetric standard models: The case of the non-universal Higgs mass model*, *PTEP* **2018** (2018), no. 2 023B06, [[arXiv:1606.04953](#)].
- [126] A. Choudhury, L. Darmé, L. Roszkowski, E. M. Sessolo, and S. Trojanowski, *Muon $g - 2$ and related phenomenology in constrained vector-like extensions of the MSSM*, *JHEP* **05** (2017) 072, [[arXiv:1701.08778](#)].

- [127] A. Choudhury, S. Rao, and L. Roszkowski, *Impact of LHC data on muon $g - 2$ solutions in a vectorlike extension of the constrained MSSM*, *Phys. Rev. D* **96** (2017), no. 7 075046, [[arXiv:1708.05675](#)].
- [128] Z. Altın, O. Özdal, and C. S. Un, *Muon $g-2$ in an alternative quasi-Yukawa unification with a less fine-tuned seesaw mechanism*, *Phys. Rev. D* **97** (2018), no. 5 055007, [[arXiv:1703.00229](#)].
- [129] W. Kotlarski, D. Stöckinger, and H. Stöckinger-Kim, *Low-energy lepton physics in the MRSSM: $(g - 2)_\mu$, $\mu \rightarrow e\gamma$ and $\mu \rightarrow e$ conversion*, *JHEP* **08** (2019) 082, [[arXiv:1902.06650](#)].
- [130] M. Endo and W. Yin, *Explaining electron and muon $g - 2$ anomaly in SUSY without lepton-flavor mixings*, *JHEP* **08** (2019) 122, [[arXiv:1906.08768](#)].
- [131] M. Badziak and K. Sakurai, *Explanation of electron and muon $g - 2$ anomalies in the MSSM*, *JHEP* **10** (2019) 024, [[arXiv:1908.03607](#)].
- [132] E. Kpatcha, I. n. Lara, D. E. López-Fogliani, C. Muñoz, and N. Nagata, *Explaining muon $g - 2$ data in the $\mu\nu$ SSM*, *Eur. Phys. J. C* **81** (2021), no. 2 154, [[arXiv:1912.04163](#)].
- [133] S. Heinemeyer, E. Kpatcha, I. n. Lara, D. E. López-Fogliani, C. Muñoz, and N. Nagata, *The new $(g - 2)_\mu$ result and the $\mu\nu$ SSM*, *Eur. Phys. J. C* **81** (2021), no. 9 802, [[arXiv:2104.03294](#)].
- [134] R. Nagai and N. Yokozaki, *Lepton flavor violations in SUSY models for muon $g - 2$ with right-handed neutrinos*, *JHEP* **01** (2021) 099, [[arXiv:2007.00943](#)].
- [135] W. Yin and M. Yamaguchi, *Muon $g - 2$ at multi-TeV muon collider*, [arXiv:2012.03928](#).
- [136] J.-L. Yang, T.-F. Feng, and H.-B. Zhang, *Electron and muon $(g - 2)$ in the B-LSSM*, *J. Phys. G* **47** (2020), no. 5 055004, [[arXiv:2003.09781](#)].
- [137] C. Han, M. L. López-Ibañez, A. Melis, O. Vives, L. Wu, and J. M. Yang, *LFV and $(g-2)$ in non-universal SUSY models with light higgsinos*, *JHEP* **05** (2020) 102, [[arXiv:2003.06187](#)].

- [138] W. Yin, *Radiative lepton mass and muon $g - 2$ with suppressed lepton flavor and CP violations*, [arXiv:2103.14234](#).
- [139] W. Yin, *Muon $g - 2$ anomaly in anomaly mediation*, *JHEP* **06** (2021) 029, [[arXiv:2104.03259](#)].
- [140] J. Cao, J. Lian, L. Meng, Y. Yue, and P. Zhu, *Anomalous muon magnetic moment in the inverse seesaw extended next-to-minimal supersymmetric standard model*, *Phys. Rev. D* **101** (2020), no. 9 095009, [[arXiv:1912.10225](#)].
- [141] J. Cao, Y. He, J. Lian, D. Zhang, and P. Zhu, *Electron and muon anomalous magnetic moments in the inverse seesaw extended NMSSM*, *Phys. Rev. D* **104** (2021), no. 5 055009, [[arXiv:2102.11355](#)].
- [142] J. Cao, J. Lian, Y. Pan, D. Zhang, and P. Zhu, *Improved $(g - 2)_\mu$ Measurement and Singlino dark matter in the general NMSSM*, [arXiv:2104.03284](#).
- [143] H.-B. Zhang, C.-X. Liu, J.-L. Yang, and T.-F. Feng, *Muon anomalous magnetic dipole moment in the $\mu\nu$ SSM*, [arXiv:2104.03489](#).
- [144] M. Endo, K. Hamaguchi, S. Iwamoto, and T. Kitahara, *Supersymmetric interpretation of the muon $g - 2$ anomaly*, *JHEP* **07** (2021) 075, [[arXiv:2104.03217](#)].
- [145] W. Ahmed, I. Khan, J. Li, T. Li, S. Raza, and W. Zhang, *The Natural Explanation of the Muon Anomalous Magnetic Moment via the Electroweak Supersymmetry from the GmSUGRA in the MSSM*, [arXiv:2104.03491](#).
- [146] S. Baum, M. Carena, N. R. Shah, and C. E. M. Wagner, *The Tiny $(g-2)$ Muon Wobble from Small- μ Supersymmetry*, [arXiv:2104.03302](#).
- [147] M. Abdughani, Y.-Z. Fan, L. Feng, Y.-L. S. Tsai, L. Wu, and Q. Yuan, *A common origin of muon $g-2$ anomaly, Galaxy Center GeV excess and AMS-02 anti-proton excess in the NMSSM*, *Sci. Bull.* **66** (2021) 1545, [[arXiv:2104.03274](#)].
- [148] M. Ibe, S. Kobayashi, Y. Nakayama, and S. Shirai, *Muon $g - 2$ in Gauge Mediation without SUSY CP Problem*, [arXiv:2104.03289](#).
- [149] M. Van Beekveld, W. Beenakker, M. Schutten, and J. De Wit, *Dark matter, fine-tuning and $(g - 2)_\mu$ in the pMSSM*, *SciPost Phys.* **11** (2021), no. 3 049, [[arXiv:2104.03245](#)].

- [150] P. Cox, C. Han, and T. T. Yanagida, *Muon $g - 2$ and Co-annihilating Dark Matter in the MSSM*, [arXiv:2104.03290](#).
- [151] C. Han, *Muon $g-2$ and CP violation in MSSM*, [arXiv:2104.03292](#).
- [152] Y. Gu, N. Liu, L. Su, and D. Wang, *Heavy bino and slepton for muon $g-2$ anomaly*, *Nucl. Phys. B* **969** (2021) 115481, [[arXiv:2104.03239](#)].
- [153] F. Wang, L. Wu, Y. Xiao, J. M. Yang, and Y. Zhang, *GUT-scale constrained SUSY in light of new muon $g-2$ measurement*, *Nucl. Phys. B* **970** (2021) 115486, [[arXiv:2104.03262](#)].
- [154] A. Aboubrahim, M. Klasen, and P. Nath, *What the Fermilab muon $g - 2$ experiment tells us about discovering supersymmetry at high luminosity and high energy upgrades to the LHC*, *Phys. Rev. D* **104** (2021), no. 3 035039, [[arXiv:2104.03839](#)].
- [155] J.-L. Yang, H.-B. Zhang, C.-X. Liu, X.-X. Dong, and T.-F. Feng, *Muon $(g - 2)_\mu$ in the B -LSSM*, [arXiv:2104.03542](#).
- [156] P. Athron, C. Balázs, D. H. Jacob, W. Kotlarski, D. Stöckinger, and H. Stöckinger-Kim, *New physics explanations of a_μ in light of the FNAL muon $g - 2$ measurement*, [arXiv:2104.03691](#).
- [157] W. Altmannshofer, S. A. Gadam, S. Gori, and N. Hamer, *Explaining $(g - 2)_\mu$ with Multi-TeV Sleptons*, [arXiv:2104.08293](#).
- [158] Z.-N. Zhang, H.-B. Zhang, J.-L. Yang, S.-M. Zhao, and T.-F. Feng, *Higgs boson decays with lepton flavor violation in the $B - L$ symmetric SSM*, *Phys. Rev. D* **103** (2021), no. 11 115015, [[arXiv:2105.09799](#)].
- [159] Z. Li, G.-L. Liu, F. Wang, J. M. Yang, and Y. Zhang, *Gluino-SUGRA scenarios in light of FNAL muon $g-2$ anomaly*, [arXiv:2106.04466](#).
- [160] P. S. Bhupal Dev, A. Soni, and F. Xu, *Hints of Natural Supersymmetry in Flavor Anomalies?*, [arXiv:2106.15647](#).
- [161] J. S. Kim, D. E. Lopez-Fogliani, A. D. Perez, and R. R. de Austri, *The new $(g - 2)_\mu$ and Right-Handed Sneutrino Dark Matter*, [arXiv:2107.02285](#).

- [162] J. Ellis, J. L. Evans, N. Nagata, D. V. Nanopoulos, and K. A. Olive, *Flipped $g_\mu - 2$* , [arXiv:2107.03025](#).
- [163] S.-M. Zhao, L.-H. Su, X.-X. Dong, T.-T. Wang, and T.-F. Feng, *Study muon $g-2$ at two loop level in the $U(1)_X$ SSM*, [arXiv:2107.03571](#).
- [164] M. Frank, Y. Hiçyılmaz, S. Mondal, O. Özdal, and C. S. Ün, *Electron and muon magnetic moments and implications for dark matter and model characterisation in non-universal $U(1)'$ supersymmetric models*, [arXiv:2107.04116](#).
- [165] S. Li, Y. Xiao, and J. M. Yang, *Can electron and muon $g - 2$ anomalies be jointly explained in SUSY?*, [arXiv:2107.04962](#).
- [166] A. Aboubrahim, M. Klasen, P. Nath, and R. M. Syed, *Future searches for SUSY at the LHC post Fermilab $(g - 2)_\mu$* , 7, 2021. [arXiv:2107.06021](#).
- [167] Y. Nakai, M. Reece, and M. Suzuki, *Supersymmetric alignment models for $(g - 2)_\mu$* , *JHEP* **10** (2021) 068, [[arXiv:2107.10268](#)].
- [168] S. Li, Y. Xiao, and J. M. Yang, *Constraining CP-phases in SUSY: an interplay of muon/electron $g - 2$ and electron EDM*, [arXiv:2108.00359](#).
- [169] W. Ke and P. Slavich, *Higgs-mass constraints on a supersymmetric solution of the muon $g-2$ anomaly*, [arXiv:2109.15277](#).
- [170] J. Rosiek, *Complete Set of Feynman Rules for the Minimal Supersymmetric Extension of the Standard Model*, *Phys. Rev. D* **41** (1990) 3464.
- [171] J. Rosiek, *Complete set of Feynman rules for the MSSM: Erratum*, [hep-ph/9511250](#).
- [172] S. Weinberg, *Supersymmetry at Ordinary Energies. 1. Masses and Conservation Laws*, *Phys. Rev. D* **26** (1982) 287.
- [173] N. Sakai and T. Yanagida, *Proton Decay in a Class of Supersymmetric Grand Unified Models*, *Nucl. Phys. B* **197** (1982) 533.
- [174] **CDF** Collaboration, T. Aaltonen et al., *Search for R-parity Violating Decays of τ Sneutrinos to $e\mu$, $\mu\tau$, and $e\tau$ Pairs in $p\bar{p}$ Collisions at $\sqrt{s} = 1.96$ TeV*, *Phys. Rev. Lett.* **105** (2010) 191801, [[arXiv:1004.3042](#)].

- [175] **D0** Collaboration, V. M. Abazov et al., *Search for sneutrino Production in $e\mu$ Final States in 5.3 fb^{-1} of $p\bar{p}$ Collisions at $\sqrt{s} = 1.96\text{ TeV}$* , *Phys. Rev. Lett.* **105** (2010) 191802, [[arXiv:1007.4835](#)].
- [176] **ATLAS** Collaboration, G. Aad et al., *Search for a Heavy Neutral Particle Decaying to $e\mu$, $e\tau$, or $\mu\tau$ in pp Collisions at $\sqrt{s} = 8\text{ TeV}$ with the ATLAS Detector*, *Phys. Rev. Lett.* **115** (2015), no. 3 031801, [[arXiv:1503.04430](#)].
- [177] **CMS** Collaboration, V. Khachatryan et al., *Search for lepton flavour violating decays of heavy resonances and quantum black holes to an $e\mu$ pair in proton-proton collisions at $\sqrt{s} = 8\text{ TeV}$* , *Eur. Phys. J. C* **76** (2016), no. 6 317, [[arXiv:1604.05239](#)].
- [178] **ATLAS** Collaboration, M. Aaboud et al., *Search for new phenomena in different-flavour high-mass dilepton final states in pp collisions at $\sqrt{s} = 13\text{ TeV}$ with the ATLAS detector*, *Eur. Phys. J. C* **76** (2016), no. 10 541, [[arXiv:1607.08079](#)].
- [179] **ATLAS** Collaboration, M. Aaboud et al., *Search for lepton-flavor violation in different-flavor, high-mass final states in pp collisions at $\sqrt{s} = 13\text{ TeV}$ with the ATLAS detector*, *Phys. Rev. D* **98** (2018), no. 9 092008, [[arXiv:1807.06573](#)].
- [180] **CMS** Collaboration, A. M. Sirunyan et al., *Search for lepton-flavor violating decays of heavy resonances and quantum black holes to $e\mu$ final states in proton-proton collisions at $\sqrt{s} = 13\text{ TeV}$* , *JHEP* **04** (2018) 073, [[arXiv:1802.01122](#)].
- [181] **ATLAS** Collaboration, B. Le, *Search for lepton flavour violation with the ATLAS experiment*, *SciPost Phys. Proc.* **1** (2019) 020.
- [182] **ATLAS** Collaboration, M. Aaboud et al., *Search for supersymmetry in events with four or more leptons in $\sqrt{s} = 13\text{ TeV}$ pp collisions with ATLAS*, *Phys. Rev. D* **98** (2018), no. 3 032009, [[arXiv:1804.03602](#)].
- [183] **ATLAS** Collaboration, M. Aaboud et al., *Search for lepton-flavor violation in different-flavor, high-mass final states in pp collisions at $\sqrt{s} = 13\text{ TeV}$ with the ATLAS detector*, *Phys. Rev. D* **98** (2018), no. 9 092008, [[arXiv:1807.06573](#)].
- [184] **ATLAS** Collaboration, G. Aad et al., *Search for supersymmetry in events with four or more charged leptons in 139 fb^{-1} of $\sqrt{s} = 13\text{ TeV}$ pp collisions with the ATLAS detector*, [arXiv:2103.11684](#).

- [185] M. Hirsch, M. A. Diaz, W. Porod, J. C. Romao, and J. W. F. Valle, *Neutrino masses and mixings from supersymmetry with bilinear R parity violation: A Theory for solar and atmospheric neutrino oscillations*, *Phys. Rev. D* **62** (2000) 113008, [[hep-ph/0004115](#)]. [Erratum: *Phys.Rev.D* 65, 119901 (2002)].
- [186] I. Esteban, M. Gonzalez-Garcia, A. Hernandez-Cabezudo, M. Maltoni, and T. Schwetz, *Global analysis of three-flavour neutrino oscillations: synergies and tensions in the determination of θ_{23} , δ_{CP} , and the mass ordering*, *JHEP* **01** (2019) 106, [[arXiv:1811.05487](#)].
- [187] P. Bhupal Dev, S. Mondal, B. Mukhopadhyaya, and S. Roy, *Phenomenology of Light Sneutrino Dark Matter in cMSSM/mSUGRA with Inverse Seesaw*, *JHEP* **09** (2012) 110, [[arXiv:1207.6542](#)].
- [188] J. Chang, K. Cheung, H. Ishida, C.-T. Lu, M. Spinrath, and Y.-L. S. Tsai, *A supersymmetric electroweak scale seesaw model*, *JHEP* **10** (2017) 039, [[arXiv:1707.04374](#)].
- [189] S. Descotes-Genon, D. Ghosh, J. Matias, and M. Ramon, *Exploring New Physics in the $C7$ - $C7'$ plane*, *JHEP* **06** (2011) 099, [[arXiv:1104.3342](#)].
- [190] T. Moroi, *The Muon anomalous magnetic dipole moment in the minimal supersymmetric standard model*, *Phys. Rev. D* **53** (1996) 6565–6575, [[hep-ph/9512396](#)]. [Erratum: *Phys.Rev.D* 56, 4424 (1997)].
- [191] J. Aebischer, J. Kumar, P. Stangl, and D. M. Straub, *A Global Likelihood for Precision Constraints and Flavour Anomalies*, *Eur. Phys. J. C* **79** (2019), no. 6 509, [[arXiv:1810.07698](#)].
- [192] **Particle Data Group** Collaboration, P. A. Zyla et al., *Review of Particle Physics*, *PTEP* **2020** (2020), no. 8 083C01.
- [193] A. J. Buras, J. Girrbach-Noe, C. Niehoff, and D. M. Straub, *$B \rightarrow K^{(*)}\nu\bar{\nu}$ decays in the Standard Model and beyond*, *JHEP* **02** (2015) 184, [[arXiv:1409.4557](#)].
- [194] J. E. Kim, P. Ko, and D.-G. Lee, *More on R-parity and lepton family number violating couplings from muon(ium) conversion, and tau and π^0 decays*, *Phys. Rev. D* **56** (1997) 100–106, [[hep-ph/9701381](#)].

- [195] B. de Carlos and P. L. White, *R-parity violation and quark flavor violation*, *Phys. Rev. D* **55** (1997) 4222–4239, [[hep-ph/9609443](#)].
- [196] M. Misiak et al., *Updated NNLO QCD predictions for the weak radiative B-meson decays*, *Phys. Rev. Lett.* **114** (2015), no. 22 221801, [[arXiv:1503.01789](#)].
- [197] **LHCb** Collaboration, R. Aaij et al., *Precise determination of the B_s^0 - \overline{B}_s^0 oscillation frequency*, [arXiv:2104.04421](#).
- [198] L. Di Luzio, M. Kirk, A. Lenz, and T. Rauh, *ΔM_s theory precision confronts flavour anomalies*, *JHEP* **12** (2019) 009, [[arXiv:1909.11087](#)].
- [199] A. Abada, M. E. Krauss, W. Porod, F. Staub, A. Vicente, and C. Weiland, *Lepton flavor violation in low-scale seesaw models: SUSY and non-SUSY contributions*, *JHEP* **11** (2014) 048, [[arXiv:1408.0138](#)].
- [200] **Top Quark Working Group** Collaboration, K. Agashe et al., *Working Group Report: Top Quark*, in *Community Summer Study 2013: Snowmass on the Mississippi*, 11, 2013. [arXiv:1311.2028](#).
- [201] **ATLAS** Collaboration, M. Aaboud et al., *Search for flavour-changing neutral current top-quark decays $t \rightarrow qZ$ in proton-proton collisions at $\sqrt{s} = 13$ TeV with the ATLAS detector*, *JHEP* **07** (2018) 176, [[arXiv:1803.09923](#)].
- [202] **ATLAS** Collaboration, G. Aad et al., *Search for flavour-changing neutral currents in processes with one top quark and a photon using 81 fb^{-1} of pp collisions at $\sqrt{s} = 13$ TeV with the ATLAS experiment*, *Phys. Lett. B* **800** (2020) 135082, [[arXiv:1908.08461](#)].
- [203] **CMS** Collaboration, V. Khachatryan et al., *Search for anomalous Wtb couplings and flavour-changing neutral currents in t-channel single top quark production in pp collisions at $\sqrt{s} = 7$ and 8 TeV*, *JHEP* **02** (2017) 028, [[arXiv:1610.03545](#)].
- [204] **ATLAS** Collaboration, M. Aaboud et al., *Search for top-quark decays $t \rightarrow Hq$ with 36 fb^{-1} of pp collision data at $\sqrt{s} = 13$ TeV with the ATLAS detector*, *JHEP* **05** (2019) 123, [[arXiv:1812.11568](#)].
- [205] J. M. Yang, B.-L. Young, and X. Zhang, *Flavor changing top quark decays in r parity violating SUSY*, *Phys. Rev. D* **58** (1998) 055001, [[hep-ph/9705341](#)].

- [206] G. Eilam, A. Geminin, T. Han, J. M. Yang, and X. Zhang, *Top quark rare decay $t \rightarrow ch$ in R -parity violating SUSY*, *Phys. Lett. B* **510** (2001) 227–235, [[hep-ph/0102037](#)].
- [207] G. Passarino and M. J. G. Veltman, *One Loop Corrections for $e^+ e^-$ Annihilation Into $\mu^+ \mu^-$ in the Weinberg Model*, *Nucl. Phys.* **B160** (1979) 151–207.
- [208] M. Beneke et al., *Top quark physics*, in *Workshop on Standard Model Physics (and more) at the LHC (First Plenary Meeting)*, 3, 2000. [hep-ph/0003033](#).
- [209] **ATLAS** Collaboration, M. Aaboud et al., *Search for B - L R -parity-violating top squarks in $\sqrt{s} = 13$ TeV pp collisions with the ATLAS experiment*, *Phys. Rev. D* **97** (2018), no. 3 032003, [[arXiv:1710.05544](#)].
- [210] **CMS** Collaboration, A. M. Sirunyan et al., *Search for long-lived particles decaying into displaced jets in proton-proton collisions at $\sqrt{s} = 13$ TeV*, *Phys. Rev. D* **99** (2019), no. 3 032011, [[arXiv:1811.07991](#)].
- [211] **ATLAS** Collaboration, M. Aaboud et al., *Search for heavy charged long-lived particles in the ATLAS detector in 36.1 fb^{-1} of proton-proton collision data at $\sqrt{s} = 13$ TeV*, *Phys. Rev. D* **99** (2019), no. 9 092007, [[arXiv:1902.01636](#)].
- [212] **ATLAS** Collaboration, G. Aad et al., *Search for long-lived, massive particles in events with a displaced vertex and a muon with large impact parameter in pp collisions at $\sqrt{s} = 13$ TeV with the ATLAS detector*, *Phys. Rev. D* **102** (2020), no. 3 032006, [[arXiv:2003.11956](#)].
- [213] **ATLAS** Collaboration, G. Aad et al., *Search for R -parity violating supersymmetry in a final state containing leptons and many jets with the ATLAS experiment using $\sqrt{s} = 13$ TeV proton-proton collision data*, [arXiv:2106.09609](#).
- [214] **CMS** Collaboration, A. M. Sirunyan et al., *Search for top squark production in fully-hadronic final states in proton-proton collisions at $\sqrt{s} = 13$ TeV*, *Phys. Rev. D* **104** (2021), no. 5 052001, [[arXiv:2103.01290](#)].
- [215] **CMS** Collaboration, A. Tumasyan et al., *Combined searches for the production of supersymmetric top quark partners in proton-proton collisions at $\sqrt{s} = 13$ TeV*, [arXiv:2107.10892](#).

- [216] **CMS** Collaboration, A. M. Sirunyan et al., *Search for supersymmetric partners of electrons and muons in proton-proton collisions at $\sqrt{s} = 13$ TeV*, *Phys. Lett. B* **790** (2019) 140–166, [[arXiv:1806.05264](#)].
- [217] **ATLAS** Collaboration, G. Aad et al., *Search for electroweak production of charginos and sleptons decaying into final states with two leptons and missing transverse momentum in $\sqrt{s} = 13$ TeV pp collisions using the ATLAS detector*, *Eur. Phys. J. C* **80** (2020), no. 2 123, [[arXiv:1908.08215](#)].
- [218] **CMS** Collaboration, A. M. Sirunyan et al., *Search for supersymmetry in final states with two oppositely charged same-flavor leptons and missing transverse momentum in proton-proton collisions at $\sqrt{s} = 13$ TeV*, *JHEP* **04** (2021) 123, [[arXiv:2012.08600](#)].
- [219] **ATLAS** Collaboration, G. Aad et al., *Searches for electroweak production of supersymmetric particles with compressed mass spectra in $\sqrt{s} = 13$ TeV pp collisions with the ATLAS detector*, *Phys. Rev. D* **101** (2020), no. 5 052005, [[arXiv:1911.12606](#)].
- [220] “Summer 2019 CKMfitter updates.” <http://ckmfitter.in2p3.fr/>.
- [221] V. De Romeri, K. M. Patel, and J. W. Valle, *Inverse seesaw mechanism with compact supersymmetry: Enhanced naturalness and light superpartners*, *Phys. Rev. D* **98** (2018), no. 7 075014, [[arXiv:1808.01453](#)].
- [222] J. S. Alvarado and R. Martinez, *PMNS matrix in a non-universal $U(1)_X$ extension to the MSSM with one massless neutrino*, [arXiv:2007.14519](#).
- [223] H. Khanpour, *Probing top quark FCNC couplings in the triple-top signal at the high energy LHC and future circular collider*, *Nucl. Phys. B* **958** (2020) 115141, [[arXiv:1909.03998](#)].